energies

MDPI

Review

Applications of 2D MXenes for Electrochemical Energy Conversion and Storage

Chenchen Ji [1,2,†], Haonan Cui [1,†], Hongyu Mi [1,*] and Shengchun Yang [3,*]

[1] School of Chemical Engineering and Technology, Xinjiang University, Urumqi 830046, China; jichenchen@xju.edu.cn (C.J.); chn954512087@stu.xju.edu.cn (H.C.)
[2] State Key Laboratory of Fine Chemicals, Dalian University of Technology, Dalian 116024, China
[3] MOE Key Laboratory for Non-Equilibrium Synthesis and Modulation of Condensed Matter, Shaanxi Province Key Laboratory of Advanced Functional Materials and Mesoscopic Physics, School of Physics, Xi'an Jiaotong University, Xi'an 710049, China
* Correspondence: mmihongyu@xju.edu.cn (H.M.); ysch1209@mail.xjtu.edu.cn (S.Y.)
† These authors contributed equally.

Abstract: As newly emerged 2D layered transition metal carbides or carbonitrides, MXenes have attracted growing attention in energy conversion and storage applications due to their exceptional high electronic conductivity, ample functional groups (e.g., -OH, -F, -O), desirable hydrophilicity, and superior dispersibility in aqueous solutions. The significant advantages of MXenes enable them to be intriguing structural units to engineer advanced MXene-based nanocomposites for electrochemical storage devices with remarkable performances. Herein, this review summarizes the current advances of MXene-based materials for energy storage (e.g., supercapacitors, lithium ion batteries, and zinc ion storage devices), in which the fabrication routes and the special functions of MXenes for electrode materials, conductive matrix, surface modification, heteroatom doping, crumpling, and protective layer to prevent dendrite growth are highlighted. Additionally, given that MXene are versatile for self-assembling into specific configuration with geometric flexibility, great efforts about methodologies (e.g., vacuum filtration, mask-assisted filtration, screen printing, extrusion printing technique, and directly writing) of patterned MXene-based composite film or MXene-based conductive ink for fabricating more types of energy storage device were also discussed. Finally, the existing challenges and prospects of MXene-based materials and growing trend for further energy storage devices are also presented.

Keywords: MXenes; energy conversion and storage; flexibility device methodologies

Citation: Ji, C.; Cui, H.; Mi, H.; Yang, S. Applications of 2D MXenes for Electrochemical Energy Conversion and Storage. *Energies* **2021**, *14*, 8183. https://doi.org/10.3390/en14238183

Academic Editor: Lyes Bennamoun

Received: 12 September 2021
Accepted: 2 December 2021
Published: 6 December 2021

1. Introduction

The increasingly prominent climate changes and limited availability of fossil fuel issues have stimulated a tremendous amount of research interest in highly efficient and clean energy storage and conversion devices [1–5]. The development of new classes of advanced two-dimensional (2D) layered materials, including graphene, MoS_2, phosphorene, have promoted tremendous technological progress in those energy resources (e.g., supercapacitor, different-type metal ion batteries (MIBs)), which are attributed to their extraordinary properties [2,6–17]. The enhancement in the performance of these devices by incorporating layered materials indicated that the 2D materials commonly possess the following two unique characteristics:

(i) The large interlayer spaces within the layered structures could provide abundant ion transport pathways, promote the ions' intercalation and diffusion, and limit the volume change during the charge/discharge process [18].
(ii) The layered structures could provide high carrier mobility [19], which ensures high electrical conductivities. Thus, 2D materials represent the most intensively and successfully investigated materials for energy storage devices.

As a novel family of transition metal carbides, carbonitrides, or nitrides, (e.g., Ti_2CT_x, Ti_3CNT_x, V_2CT_x), MXenes have attracted particular research enthusiasm since their discovery in 2011 [20]. The delaminated MXenes have elevated research on the novel 2D materials to a new era in the energy related fields due to their prominent and attractive properties, including adjustable composition, hydrophilic, conductivity, thermal conductivity, tunable band gap, and excellent mechanical strength [21–26]. However, MXenes themselves are easily to spontaneously stack and aggregate into multilayer structures due to strong van der Waals forces between the layers, which lead to the decrease in the interlayer space and sluggish kinetics for redox activities or intercalation/deintercalation behaviors [27]. Thus, the capabilities to enlarge the space between the interlayer and elaborately modulate pathways or active sites for MXenes draw lots of attention. As experienced by other 2D materials, several strategies have been proposed for successfully solving the challenges mentioned above, which includes the surface modification, heteroatom doping, or crumpling [28–33]. Recent investigation also demonstrated that the MXene are versatile for self-assembling into specific configuration with geometric flexibility [34]. In this sense, substantial efforts have also been made in methodologies of patterned MXene-based composite film or MXene-based conductive ink for fabricating more types of energy storage devices, which encompasses vacuum filtration, mask-assisted filtration, screen printing, extrusion printing technique, and directly writing, etc. In general, the materials and electrodes for various energy storage devices need to fulfill the requirements of stable physicochemical properties, superb energy storage performance, and high electron/ion conduction [35]. By now, available and optional strategies for enhancing the ion and electron transfer ability of MXene-based materials and the methodologies to design satisfactory patterns are still limited due to the primary development stage of MXenes [36–38]. It is highly needed to get intensive and systematical understanding about the progress of elaborately constructing advanced MXene-based electrode materials and versatile MXene-based flexible electrodes with favorable configurations. In this regard, the efforts on the synthetic method of MXene, the enhancement in electrochemical performance of MXene materials, and the research strategies and technologies to fabricate flexible electrodes for energy storage are briefly summarized. Meanwhile, the challenges and perspectives of MXene-based materials and technologies for the future energy storage applications are presented.

2. Synthetic Methods

The MXene flakes are commonly synthesized by using hydrofluoric acid or a mixed solution of lithium fluoride and hydrochloric acid to selectively remove the "A" layer from the ternary MAX phase, where the M represents early transition metals (e.g., Ti, Mo, V), the A represents IIIA or IVA group elements (e.g., Al, Ga, Si, Ge), and the X represents C and/or N. The MXenes usually possess accordion-like hexagonal lattices which result from the original metallic backbone, weak M-A bond, and strong M-X bond [39]. Meanwhile, some surface terminal groups (e.g., -OH, -O, -F) are formed during the bond breaking and binding processes, which provides more active sites as well as suitable interlayer spacing (Figure 1). Till now, the routinely used method for synthesizing the MXene and its derivatives is hydrofluoric acid (HF) etching. Early works revealed that HF is the most effective etchant to selectively react with the "A" layer atoms and continual out-diffusion to exfoliate the MAX phase (such as Ti_3AlC_2). Those works also proved that the MAX phases are inert in the conventional acids (e.g., H_2SO_4, HCl, and HNO_3), alkaline liquors (e.g., NaOH), and salt solutions (e.g., NaCl and Na_2SO_4). Nevertheless, HF reagent is a hazardous poison with a highly corrosive property to the human body. The direct use of HF raises the potential for causing considerable safety and environmental problems [40]. Thus, many mild etchants have been developed (e.g., NH_4HF_2, or a mixture of LiF/HCl). It was noted that the diverse routes will bring different surface functional groups such as fluoride (-F), hydroxyl (-OH), and/or oxygen (-O) on MXenes and give rise to different levels of delamination, and hence, the preparation process will directly determine the properties of the final MXenes, e.g., metallic, semi-metallic, and semiconducting types. To

understand the formation fundamentals from the MAX phase to the MXene sheets, three basic approaches will be discussed in the sections (e.g., wet-chemical etching in hydrofluoric acid, in situ HF-forming method, and freeze-and-thaw-assisted (FAT) method).

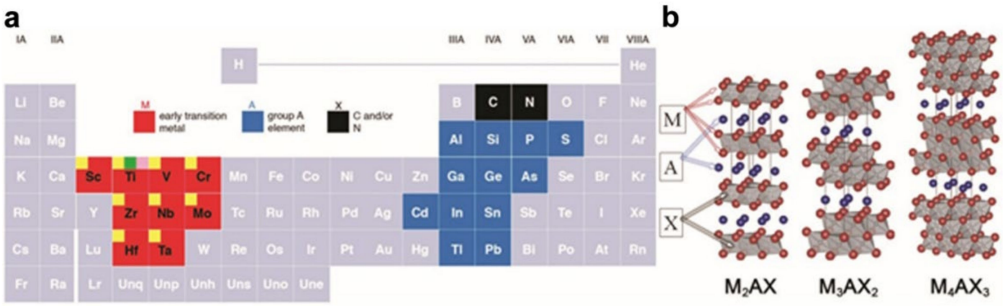

Figure 1. (**a**) The elements of the periodic table for MAX phases. (**b**) Structures of M_2AX, M_3AX_2, and M_4AX_3 phases [41].

2.1. Wet-Chemical Etching

The first MXene of Ti_3C_2 was obtained from the MAX phase of Ti_3AlC_2 in the HF solution after successful and selective removal of Al atoms. Subsequently, various kinds of MXene members have been developed by using the wet-chemical etching in hydrofluoric acid. Interestingly, after the etching, the deficiencies of the Al atoms change the structure from undamaged cube to accordion-like cube due to the stable bond between M-X and the weak bonding to the A-M layers. In addition, the as-formed Al deficiencies able to expose more Ti atoms to the atmosphere and further facilitate the exposed terminations to combine with other functional groups. Hence, the extraction processes help to vary the surface chemistries and change their band gap, which results in a higher surface chemical activity of MXene in contrast to MAX phase. The reaction formula for the selective etching process can be ascribed as following [20]:

$$Ti_3AlC_2\ (s) + HF(aq) = AlF_3(aq) + 3/2H_2(g) + Ti_3C_2\ (s) \quad (1)$$

$$Ti_3C_2(s) + 2H_2O(aq) = Ti_3C_2(OH)_2(s) + H_2(g) \quad (2)$$

$$Ti_3C_2(s) + 2HF(aq) = Ti_3C_2F_2(s) + H_2(g) \quad (3)$$

where Equation (1) represents the selective reaction of A layers with HF etchant while Equations (2) and (3) always react together and represent the growth mechanism of the function groups on the exposed Ti atoms [42].

2.2. In Situ HF-Forming Method

The in situ HF-forming strategy commonly employs fluoride-containing acidic solutions (e.g., lithium fluoride (LiF), ammonium hydrogen fluoride (NH_4HF_2), sodium bifluoride ($NaHF_2$), and potassium hydrogen fluoride (KHF_2)) [43–50] to indirectly produce HF etchants for stripping Al atoms, the reaction for the etching process can be described as the following:

$$LiF(aq) + HCl(aq) = HF(aq) + LiCl(aq) \quad (4)$$

The synthetic reaction usually occurs at 40 °C and the obtained samples need to be rinsed to remove the by-products, such as AlF_3, LiCl. However, the lower concentration of hydrogen fluoride and fluoride salts compared with HF etchants and long etching time lead to poor etching effect and the accordion-like morphology is hard to obtain in the reaction system.

2.3. Other Synthesis Method

Given that most of the commonly used synthetic methods have low exfoliation yields, some alternative and effective strategies were developed for boosting the yield of MXenes. Recently, Wu and co-workers reported a gentle water FAT method to prepare the MXene nanosheets by inserting water molecules into the multilayer of MXene and using the volume expansion process to raise the exfoliation efficiency. The yield of these FAT-MXene can reach to 39% and can further increase to 81.4% by the sonication treatment [51]. In addition, due to the water-freezing expansion force, the method can prevent the restacking and expand the space between the multilayer during the reaction process. The FAT-MXene also possesses larger flake size compared with MXenes obtained from other methods (Figure 2). Therefore, films or current-collector-free electrodes assembled from the FAT-MXene exhibit a high level of layer alignment and a low flake-to-flake contact resistance, which enables the FAT-MXene-based on-chip micro-supercapacitor to display a high areal capacitance of 23.6 mF cm^{-2} and a high volumetric capacitance of 591 F cm^{-3}.

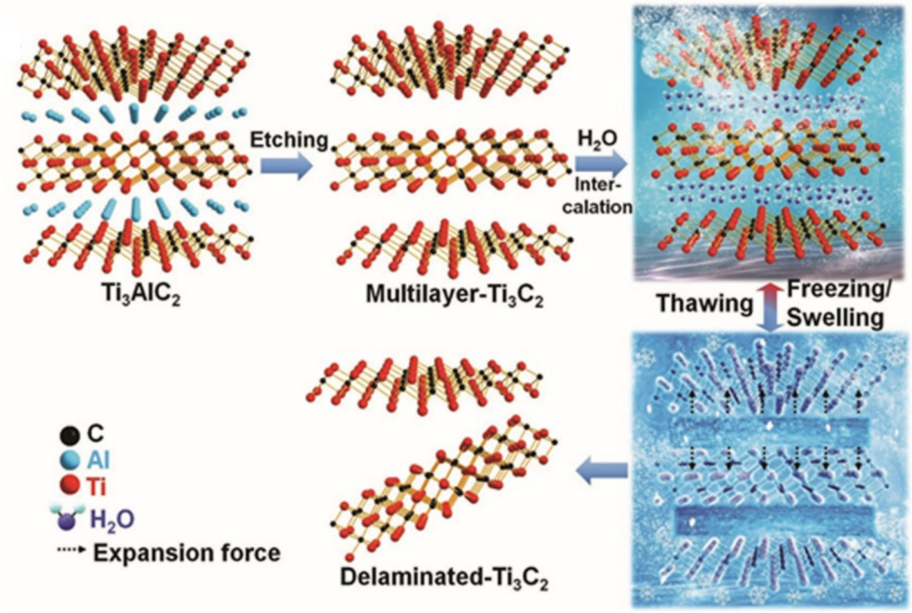

Figure 2. The synthesis process of FAT assisted method [51].

3. Electrochemical Energy Storage Applications

The electrochemical energy storage systems implement energy conversion through electrophysical process (e.g., electrosorption of ions) or electrochemical redox reactions coupled with ions and electrons migration within electrolytes and electrodes. In these systems, 2D materials, such as graphene, black phosphorene, and MoS_2 attract extensive concern due to their favorable morphological and electrical properties [52,53]. Additionally, recent advances in MXenes have enhanced the performance for storage devices (e.g., supercapacitors and metal-ion batteries) and exhibit extraordinary physical and chemical properties, such as mechanical flexibility, high tap density (4.0 g cm^{-3}), high electrical conductance (3.1×10^3 S m^{-1} for MXene and 2.0×10^3 S m^{-1} for graphene) [42,54,55], outstanding volumetric capacity (up to 1500 F cm^{-3}), and favorable hydrophilicity [56,57].

3.1. Supercapacitors (SCs)

Supercapacitors (SCs) are kinds of energy storage devices that contain negative electrodes, positive electrodes, separators, and electrolytes [58]. Normally, SCs possess significant advantages of fast charge/discharge rates, high power density, and long cycle stability due to their special energy storage mechanism. In general, SCs can be classified as electrical double-layer capacitance (EDLC), pseudocapacitors, and hybrid supercapacitors [59]. The EDLC mechanism is an electro-physical storage process that involves the charge accumu-

lation and reversible adsorption/desorption of electrolyte ions on the interface between electrodes and electrolytes [60]. The commonly used electrode materials for EDLC are mainly porous carbonaceous materials. Pseudocapacitors, also called redox capacitors, store charges via the electrochemical processes of surface redox reactions with electron gain/loss or pseudocapacitive intercalation [61]. Hybrid supercapacitors (HSC) integrate EDLC-type and redox-type electrodes in the device and display an electrophysical and electrochemical mixed mechanism [62]. The schematic illustrations of different SCs are shown in Figure 3.

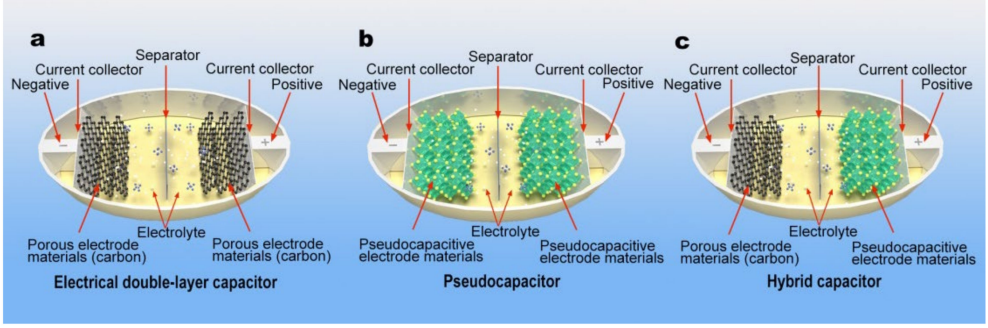

Figure 3. Schematic illustrations of (**a**) a EDLC with porous carbon materials for each electrode, (**b**) a pseudocapacitor with transition metal-related material for each electrode, and (**c**) asymmetric hybrid capacitors utilizing a porous carbon negative electrode and a transition metal oxide positive electrode.

The charge storage mechanism for MXene (e.g., $Ti_3C_2T_x$) is commonly identified as a Faraday redox processes, which involves transitions between various oxidation states of titanium during the intercalation/deintercalation processes of ions in the electrolytes [63]. Yury Gogotsi and co-workers demonstrated that the intercalation/deintercalation of cations (K^+ and NH^{4+}) from alkaline electrolyte into Ti_3C_2 MXene layers in a range of −0.6–0 V are responsible for the electrochemical performance and capacitances of these materials, and the corresponding electrochemical reaction can be ascribed as follows [55,64]:

$$Ti_3C_2T_x + \delta K^+ + \delta e^- \rightleftharpoons K_\delta Ti_3C_2T_x \quad (5)$$

The Faraday processes in a potential window of 0–0.6 V for the MXenes (e.g., Ti_3C_2) as the positive SC electrodes in alkaline electrolyte may involve the following reactions [65].

$$Ti_3C_2O_x(OH)_yF_z + \delta OH^- \rightleftharpoons Ti_3C_2O_x + \delta(OH)_y{}^-\delta F_z + \delta H_2O + \delta e^- \quad (6)$$

$$Ti_3C_2O_x + \delta OH^- \rightleftharpoons Ti_3C_2O_x(OH)_\delta + \delta e^- \quad (7)$$

MXene-based composites. In order to solve the restacking problem mentioned above and further enhance the charge storage performance of MXenes, Sun and co-workers adopted the Ti_3C_2 MXene and 1T-MoS_2 to construct a 3D interpenetrated architecture of 2D/2D 1T-MoS_2/Ti_3C_2 heterostructure by the magneto-hydrothermal method. Enhanced electrochemical performances are observed from this material, which result from the synergistically interplayed effect of the unique 3D interpenetrated heterogeneous networks (e.g., enlarged ion storage space between Ti_3C_2 and 1T-MoS_2 for storing more electrolyte ions, boosted electron conductivity provided by MXene, and more active sites for redox reaction offered from 1T-MoS_2 phase). As a result, the heterogeneous material exhibits a specific capacitance of 386.7 F g^{-1} at 1 A g^{-1} in a potential window of −0.3–0.2 V with outstanding rate performances (a high capacitance of 207.3 F g^{-1} at 50 A g^{-1}). They also reported that the total capacitance of this material comes from three parts, containing contributions originating from 1T-MoS_2, MXene, and extra H^+ storage in the interpenetrated space within the 3D heterostructure (Figure 4), while the 1T-MoS_2/MXene sample without heterostructure lacks the extra H^+ storage capacitance, indicating the existence of a strong coupled effect

between composition and structure for the 3D heterostructure. Furthermore, a symmetric SC based on the as-design material displayed a high areal capacitance of 347 mF cm^{-2} at 2 mA cm^{-2} with excellent cycle stability (91.1% capacitance retention after 20,000 cycles) (Figure 4) [66].

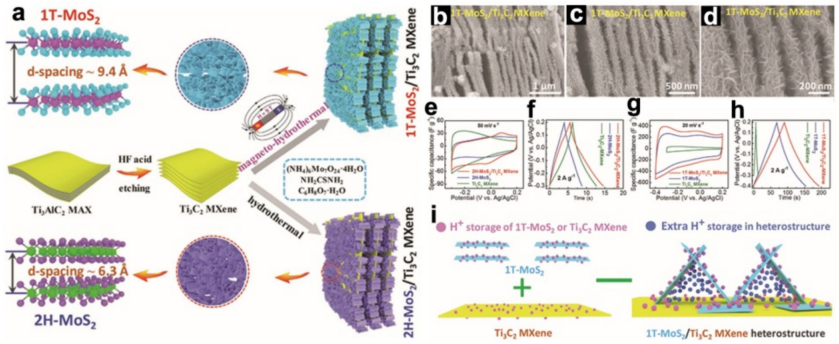

Figure 4. (**a**) Schematic illustrating the preparation process for the two types of the MoS_2/Ti_3C_2 MXene 3D heterostructures. (**b**–**d**) SEM images of the prepared 1T-MoS_2/Ti_3C_2 MXene sample. (**c**) Electrochemical performance of the prepared heterogeneous electrodes. (**e**–**h**) Electrochemical performance of the prepared samples. (**i**) Schematic diagram of the storage mechanism for the heterostructure [66].

A Ti_3C_2/CuS composite as the positive electrode in alkaline electrolyte (within a potential window of 0–0.6 V) delivers a capacity of 169.5 C g^{-1} at 1 A g^{-1} with a capacity retention of 90.5% at 5 A g^{-1} after 5000 long-term cycles. An asymmetric SC fabricated by the Ti_3C_2/CuS positive electrode and Ti_3C_2 negative electrode at a voltage range of 0–1.1 V reveals a specific capacitance of 49.3 F g^{-1} to 0–1.5 V with a maximum energy density of 15.4 Wh kg^{-1} and a capacitance retention of 82.4% after 5000 cycles [65]. A MXene/nickel-aluminum layered double hydroxide (MXene/LDH) composite in 6 M KOH aqueous electrolyte within a range of 0–0.6 V displays a specific capacitance of 1,061 F g^{-1} at 1 A g^{-1} with a retention of 70% after 4000 charge/discharge cycles [67]. A nickel sulfide/Ti_3C_2 (Ni–S/Ti_3C_2) nanohybrid in 6.0 M KOH aqueous electrolyte within a window of 0–0.6 V exhibits a capacity of 840.4 C g^{-1} with enhanced rate performance (a capacity retention of 64.3% at 30 A g^{-1}) and a long cycle life. An asymmetric SC assembled by the Ni–S/Ti_3C_2 positive electrode and Ti_3C_2 negative electrode delivers an energy density of 20.0 Wh kg^{-1} at a voltage range of 0–1.8 V and a good cycling stability (a capacity retention of 71.4% after 10,000 cycles) [68]. Doping heteroatoms (e.g., nitrogen) into the MXene structures could modify their electronic structure, composition, and pseudocapacitance properties. In addition, heteroatom-doping can also lead to a remarkable increase of the interlayer spacing between MXene flakes. As Dai and co-workers found, the c-lattice parameter of the MXene layers could increase from 1.92 to 2.46 nm after the nitrogen-doping process, indicating the doped N atoms expand the interlayer spacing of the MXene sheets. Thereby, the resultant doped materials delivered much higher capacitances of 192 F g^{-1} in 1 M H_2SO_4 within a potential range of −0.2–0.35 V than those un-doped $Ti_3C_2T_x$ materials [69].

Previous theoretical and experimental studies reveal that the chemical and physical characters of MXenes are heavily influenced by their surface functional groups. Yury Gogotsi et al. found that the MXene (e.g., $Ti_3C_2T_x$) with rich surface O-termination exhibited high surface activity and better pseudocapacitance performance [63,70]. Fan et al. enhance the electrochemical performance of MXene by using the ammonium persulfate as the weak oxidant and intercalation agent to partially remove the F terminations coupled with controllably oxidizing the $Ti_3C_2T_x$ surface to produce rich O-terminations. Recently, electrochemical test results have shown that the modified $Ti_3C_2T_x$ possess an enhanced capacitance of 303 F g^{-1} and the capacitance retention could be 96.6% after 9000 cycles [71]. MXene can also form a composite with the N, O co-doped carbon materials to expand the interlayer spacing and avoid the re-stacking problems of the MXene sheets. Due to

these reasons, a N, O co-doped carbon@MXene composite exhibited a higher specific capacitance of 250.6 F g^{-1} at 1 A g^{-1} compared with pristine Ti_3C_2 and retained 94% of its initial capacitance after 5000 cycles. Furthermore, a symmetric SC based on this composite electrode displayed an excellent electrochemical performance with an energy density of 10.8 Wh kg^{-1} at 600 W kg^{-1} and desirable cycling stability [28]. Zhenxing Li's group synthesized a dodecaborate/MXene highly conductive composite by surface modified with ammonium ion and inserted the dodecaborate ion into the inner surface of MXene via the electrostatic adsorption. The delocalized negative charge of dodecaborate ion facilitates the cations transfer, which efficiently boosted the ion transfer rate during the charge storage process due to its "lubricant" effect for electrolyte ions. Due to the above reasons, a high specific capacitance of 366 F·g^{-1} can be obtained at 2 mV·s^{-1} [72].

Among all other pseudocapacitive materials, MXenes offer ultrahigh rate capability, excellent conductivity, and volumetric capacitance in SC applications. Actually, MXenes and most MXenes-derived composites commonly are only served as negative electrode materials as their easy oxidation feature at positive potential (anodic oxidation process). To further enhance its antioxidant performance at positive potential, some works tried to improve the work function (WF) of the final product by means of compounding. For instance, Gogotsi and co-workers reported a PANI@MXene cathode material by evenly covering an oxidation resistive PANI layer on the surface of MXene network. The first principle calculation results manifested that the PANI with a large WF (WF = 3.46 eV, the WF for metallic MXene is 1.61 eV) effectively expanded the WF of the composite to 1.97 eV by forming a compact PANI@MXene heterostructure, which helps to enhance the electrochemical stability at a wider positive operating potential (0–0.6 V). Therefore, the as-formed PANI@MXene composite can be used as a positive electrode for steady energy storage with a high volumetric capacitance of 1632 F cm^{-3} and a desirable rate capability. They also claimed that the asymmetric SC assembled by MXene anode and PANI@MXene cathode delivered a volumetric energy density of 50.6 Wh L^{-1} with an ultrahigh volumetric power density of 127 kW L^{-1}. This work also reasonably suggested that other materials (e.g., inorganic compounds or macromolecule materials) with higher WF may enhance the resistance of losing electrons at positive potentials and enlarge the operation working windows for MXenes via forming MXene-based composites [73].

Flexible MXene thin films or free-standing electrodes. It is well known that MXenes are simultaneously capable of conducting electrons and storing charges. In addition, they also possess the compatible structural properties of flexibility, self-assembly, and miniaturization. Meanwhile, the functionality of the MXene macroscopic films or assemblies could be further improved through further optimizing the MXene synthesis conditions, tuning the MXene interlayer spacing, altering the types or amount of surface terminations, controlling the size and thickness of MXene flakes, and compositing with other functional materials (e.g., metal organic framework), and therefore, it is reasonable to suppose that the $Ti_3C_2T_x$ can be used as free-standing electrodes for SC devices with more functionality. Nicolosi and co-workers adopted a spin-casting method to produce highly aligned and transparent continuous $Ti_3C_2T_x$ film, which displays remarkable optoelectronic performances, e.g., bulk-like conductivity, high transmittance, and desirable pseudocapacitance performances. Owing to the structural and electronic properties, the as-designed $Ti_3C_2T_x$ electrodes could function as both active materials and transparent current collector for SCs. Meanwhile, they also found that the as-designed energy devices exhibit high areal/volumetric capacitances with superior energy/power densities and long cycle life [74], demonstrating the application potential for optoelectronics and flexible electronics of MXene materials.

The existence of surface terminations on the MXene sheets are beneficial to form strong bonds between MXenes and specific materials, which help to boost the electrical conductivity and structural/electrochemical stabilities of the active components and the final films. Huang and co-workers employed a vacuum-assisted filtration method to construct the MXene/metal-porphyrin frameworks (MPFs) hybrid flexible free-standing film via forming the interlayer hydrogen bond between the electronegative surface (results from the

functional groups of -O, -F, or -OH) of MXene and hydrogen atom of carboxy terminations (-COOH) in MPFs. The composite electrode with interconnected conductive networks and interlayer hydrogen bonds (e.g., F···H-O and O···H-O) eliminated the inferior conductivity and low structural stability problems of MPFs, showing favorable flexibility, high ionic/electronic transport rates, and durability. Meanwhile, the as-designed MXene/MPFs film can normally operate in a potential window of −0.3–0.3 V (vs. Ag/AgCl) and exhibits a specific capacitance of 326.1 F g^{-1} and excellent durability. In addition, a flexible symmetric SC fabricated by the MXene/MPFs film delivers an areal capacitance of 408 mF cm^{-2} and an areal energy density of 20.4 μWh cm^{-2} with a long term stability of 7000 cycles (with a capacitance retention of 95.9%). This work also indicated that the formation of interlayer hydrogen bond between MXene and other components contributes to enhance the chemical stability by effectively avoiding the phase separation or structural collapse problems of the electrode materials during the energy storage processes (Figure 5) [75]. Wu et al. used the Buchwald-hartwig coupling reaction to prepare a decentralized conjugated polymer (PDT)/$Ti_3C_2T_x$ hybrid flexible freestanding film via an electrophoretic deposition and the following spin coating processes. Similarly, they found that a stable chemical bond (e.g., hydrogen bonds) can be formed between the terminal groups of the $Ti_3C_2T_x$ sheets and the decentralized chains of PDTs, which enables the final polymer matrix composite film to effectively relieve the volumetric swelling and shrinking problems of polymer chains during the charge/discharge processes [76].

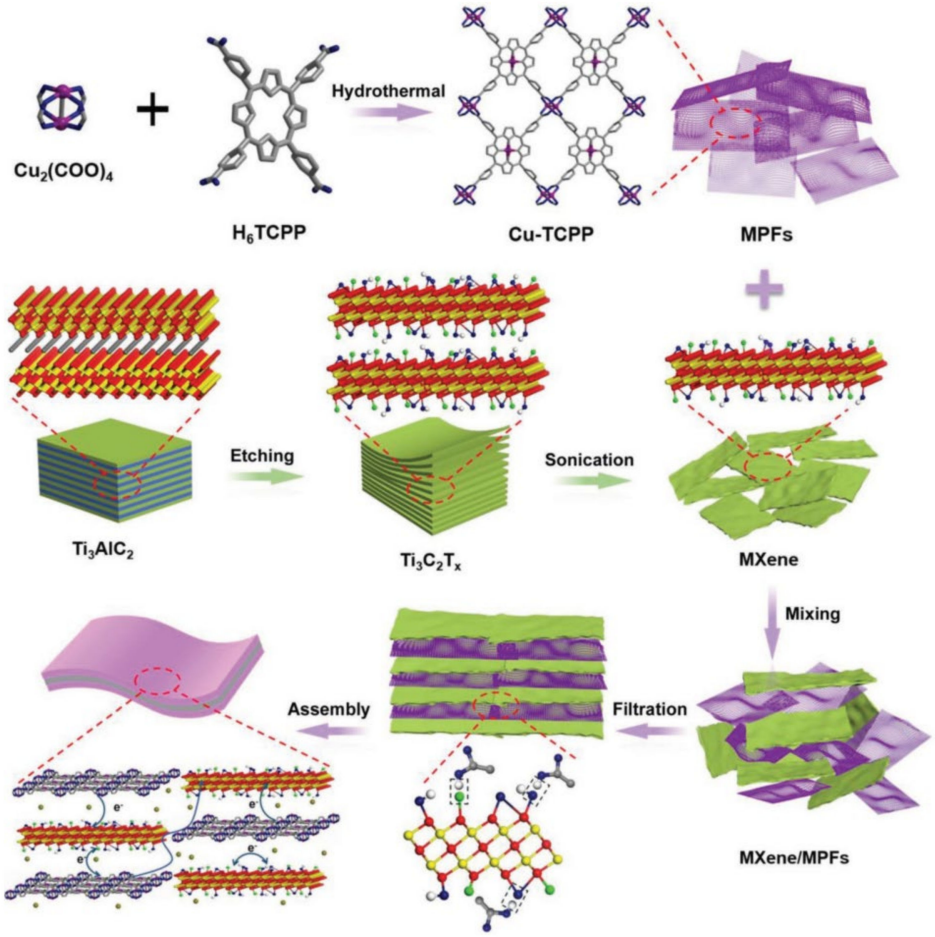

Figure 5. Schematic illustration of the synthesis process for the MXene/MPFs film via interlayer hydrogen bond [75].

The delaminated MXene flakes with monatomic or few-atom-layer thicknesses have shown their capabilities to assemble free-standing and flexible films with outstanding

electronic conductivity and excellent electrochemical performance due to their 2D lamellar structures, abundant surface functional groups, and remarkable charge transfer capabilities. Nevertheless, the propensity for "face to face" horizontal stacking with less open tunnels reduces the interlayer space between isolating MXene flakes and suppresses electrolyte ions transport or intercalation, which limits their potential in electrochemical storage applications. Therefore, opportunities to control the MXene nanosheets alignment, especially through designing unique architectures to tune the porosity, expanding the interlayer spacing, and manipulating the surface functional groups, need to be further explored. In order to alleviate the stacking problems of MXenes, Zheng et al. employed the vacuum filtration method with the assistance of entwined metal mesh to control the alignment of MXene sheets and fabricate an "anti-T-shape" MXene film electrode. They claimed that the unique "magazine-bending" structure facilitated the vertical electrolyte ion transport and enhanced the kinetics of the electrochemical process which enable the "anti-T-shape" electrodes in a symmetric SC to display a low interfacial impedance, a high pseudocapacity of 194 F g^{-1}, superior energy/power densities of 11.27 Wh kg^{-1}/699.9 W kg^{-1}, and a favorable capacitance retention of 70.3% after 10,000 cycles [31].

Zhang's group utilized the vacancy ordered $Mo_{1.33}C$ MXene and poly(3,4-ethylenedioxythiophene):poly(styrenesulfonic acid) (PEDOT:PSS) to fabricate the flexible aligned $Mo_{1.33}C$ MXene/PEDOT:PSS composite films by a vacuum filtration process. The electrochemical test results show that the MXene-based films with the optimal ingredients ratio (the mass ratio between $Mo_{1.33}C$ MXene and PEDOT:PSS is 10:1) display a high conductivity of 29,674 S m^{-1} and a maximum volumetric capacitance of 1,310 F cm^{-3} in the potential range from −0.35 to 0.3 V in 1 M H_2SO_4 aqueous electrolyte, which may result from the synergistic effect of expanded interlayer spacing of MXene sheets caused by the PEDOT component and the extra redox activity of the PEDOT. Due to these reasons, a maximum volumetric capacitance of 568 F cm^{-3} and energy density of 33.2 mWh cm^{-3} can be obtained for the film-based flexible all-solid-state SC [77].

The performances and surface chemistries of the MXene film electrode can be further tuned by compositing with various functional nanomaterials or in different types of electrolytes. Xingbin Yan's group adopted the MXene (Ti_3C_2) as charge-transfer pathways and graphite carbon nitride (g-C_3N_4) as the ion-accessible channels to construct a 2D heterogeneous nanospace for dual confining the FeOOH quantum dots via a vacuum filtration to fabricate a freestanding FQDs/CNTC film electrode, which shows superior pseudocapacitive performances with favorable kinetics in a high-voltage ionic liquid (IL) electrolyte (1-ethyl-3-methylimidazolium tetrafluoroborate, abbr., $EMIMBF_4$). The test results indicated that the surface functional groups of Ti_2C_3 and active sites (e.g., N defects) of the g-C_3N_4 in the FQDs/CNTC electrode are crucial for offering sufficient redox reaction by efficiently forming the strong adsorption between the electrolyte ions and the electrode interface (Figure 6a). Furthermore, a 3 V flexible SC was constructed in the IL electrolyte, which exhibited volume energy/power densities of 77.12 mWh cm^{-3}/6000 mW cm^{-3}, and desirable flexible cycling performance (Figure 6b,c) [78]. The as-obtained FQDs/CNTC film based flexible SC can easily power portable electronics under complex motion states (Figure 6d) or store solar energy (Figure 6e), showing a new insight into construction of MXene-based composite film electrode and flexible SC.

Mahiar M. Hamedi's group prepared MXene-based freestanding films via a vacuum filtration by using the carboxymethylated cellulose nanofibrils (CNFs) as functional additive to strengthen the mechanical properties of the films. A hybrid film with a 10% CNF loading displays a high Young's modulus (41.9 GPa), a high mechanical strength (154 MPa), a high electric conductivity (690 S cm^{-1}), and a high specific capacitance (325 F g^{-1}), which shows great potential for flexible functional electronics. They claimed that the superior properties root in the strong interfacial interactions between $Ti_3C_2T_x$ flakes and CNF (Figure 7) [79].

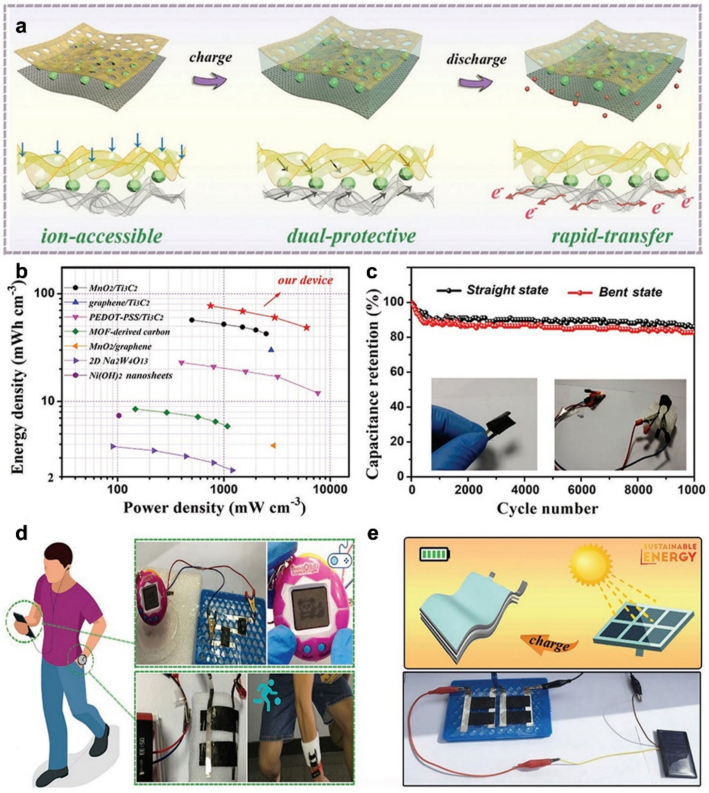

Figure 6. (**a**) Schematic illustration of the charge-discharge processes for FQDs/CNTC film electrode. (**b**) Ragone plot of the as-designed flexible SC. (**c**) Cycling performance of the flexible SC under the bent state. (**d**) Digital photos of the flexible SCs power diverse portable electronics. (**e**) Schematic of the flexible SC charged by harvesting solar energy [78].

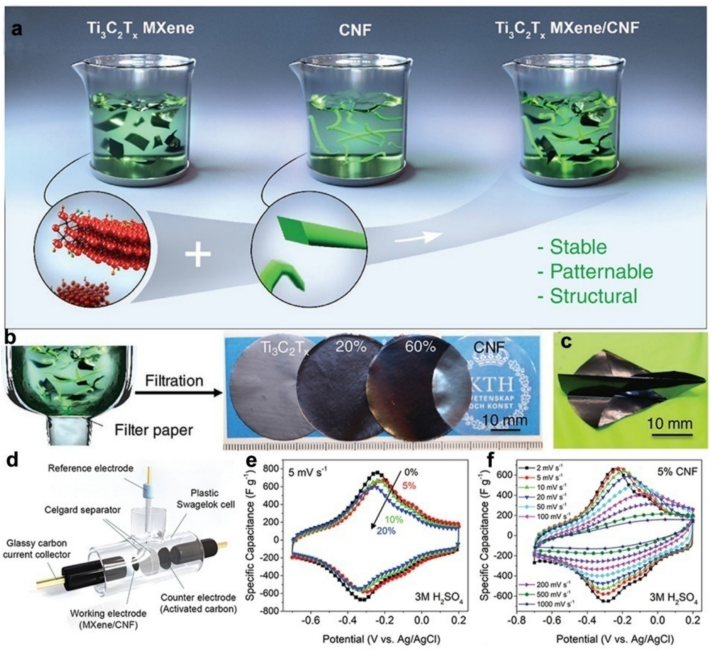

Figure 7. (**a**) Schematics of $Ti_3C_2T_x$/CNF hybrid dispersion. (**b**) The synthesis method and digital photographs of $Ti_3C_2T_x$/CNF nanopapers. (**c**) Photos of a $Ti_3C_2T_x$/CNF nanopaper. (**d**) Schematic of the three-electrode system in this work. (**e**) CV curves of MXene with different ratio of CNF. (**f**) CV curve of $Ti_3C_2T_x$–5% CNF electrode at various scan rates [79].

Given the interconnected networks and high tensile strength, bacterial cellulose (BC) was confirmed as excellent spacers for loading MXene to construct robust film electrodes with strong mechanical strength. In this regard, Guohui Yuan's group prepared a 3D self-supporting film electrode comprising interconnected MXene and BC networks. Due to excellent electron conductivity, large ion-accessible active sites, effective ion diffusion, and robust mechanical properties of the MXene/BC network, the as-obtained film electrode exhibits a high capacitance (416 F g^{-1}, 2084 mF cm^{-2}) coupled with excellent mechanical performance. Moreover, an ultrahigh energy density of 252 μWh cm^{-2} can be obtained in an asymmetric SC, which provided a simple route for fabricating high performance film electrodes in energy storage fields [80].

MXene inks and printable microsupercapacitor (MSC). To date, various construction methodologies to manufacture versatile micro-power systems have been developed. Among them, printing (e.g., laser printing, direct writing, screen printing, and extrusion printing) has been regarded as one of the most revolutionary techniques to construct functional energy storage devices with designed or desirable patterning. MXenes can also be used as attractive printing materials (e.g., conductive inks), which are essential for realizing the fabrication of geometric flexible, printable, and free-standing electrochemical devices. Thus, many works focus on the design of certain formulations of MXene conductive inks for achieving higher compatibility with various patterning methods. In addition, many simple and affordable strategies to obtain the MXene-based coplanar interdigital electrodes for further assembling into printable or direct-write SC devices are progressively developed, which shows extra advances in their versatility, high resolution patterning, simplicity, and desirable performances. Many previous works also indicated that some of the existing micro fabrication techniques often require sophisticated instrumentation and tedious multistep manufacturing processing, and therefore, MXenes inks or MXene-based coplanar electrodes and the corresponding printing techniques exhibit exciting potential for manufacturing of low-cost and easily processing printable electronics.

Yury Gogotsi and co-workers adopted simple and additive-free formulations to prepare solution processable MXene-in-water (e.g., Ti_3C_2) inks, which can be loaded in pens to direct write conductive MXene electrical circuits and desired shape either by manual drawing or automatic drawing tools on a variety of substrates (e.g., printer paper and polypropylene membranes) for functional energy storage devices. The developed MXene versatile inks are also compatible with other patterns, such as stamping, printing, and painting. Additionally, the as-written MXene collector-free MSC as power sources display an areal capacitance of 5 mF cm^{-2}, and a tandem device can drive a LED to operate normally, demonstrating the practical application of this technique (Figure 8) [81].

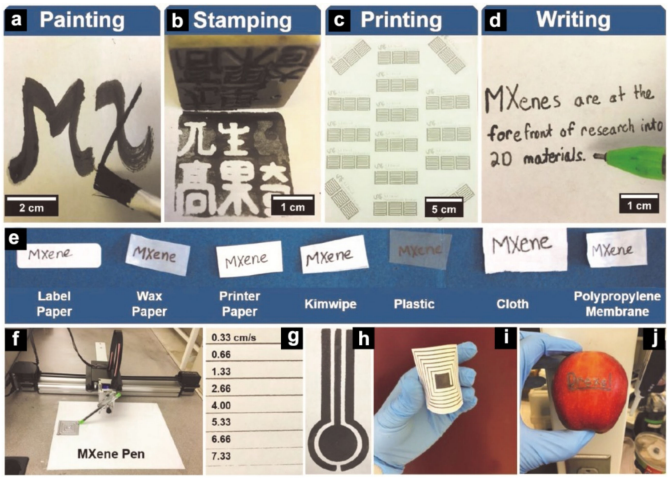

Figure 8. (**a**–**e**) Written MXene on various substrates via various ways, (**f**,**g**) using the automatic drawing tool of AxiDraw for patterning by using the Ti_3C_2 inks, (**h**,**i**) versatile patterning using AxiDraw, and (**j**) a demonstration of MXene inks drawn on an apple [81].

Screen printing and extrusion printing are two kinds of versatile direct printing techniques to fabricate the SC electrodes or MSC devices with geometric flexibility and desirable architectures. Screen printing is widely used to build up 2D flexible or wearable electronics due to its scalable and facile property, while extrusion printing could implement customized 3D printing through digital processing. In a manner, the rheological properties of the employed inks are pivotal for realizing the different printing modes. Commonly, extrusion printing requires more viscous inks compared to screen printing for keeping the 3D architectures from collapsing [56]. MXenes or their derivates could develop certain functional conductive inks for printed energy storage devices due to their intrinsic favorable hydrophilicity, mechanical flexibility, and modifiability [82]. Sun and co-workers used the melamine formaldehyde as the template to develop the crumpled heteroatom nitrogen-doped MXene flakes (MXene-N). They also found that the nitrogen doping effectively boosts the conductivity and electrochemical activity of the MXene flakes. Accordingly, two kinds of MXene-N inks (e.g., binder-additive aqueous ink and binder-free hybrid ink) are developed via optimizing the viscosity for screen printing and extrusion printing, respectively. The obtained screen printed flexible MXene-N based MSCs display an areal capacitance of 70.1 mF cm^{-2}. The as-fabricated 3D extrusion printed SC using the hybrid ink that includes the N-doping MXene, AC, CNT, and GO, delivers an areal capacitance of 8.2 F cm^{-2} with an areal energy density of 0.42 mWh cm^{-2}. This work also proposed a versatile solution to relieve the restacking issues of MXene flakes within the printed electrodes for further facilitating the ion/electrolyte transport (Figure 9) [56].

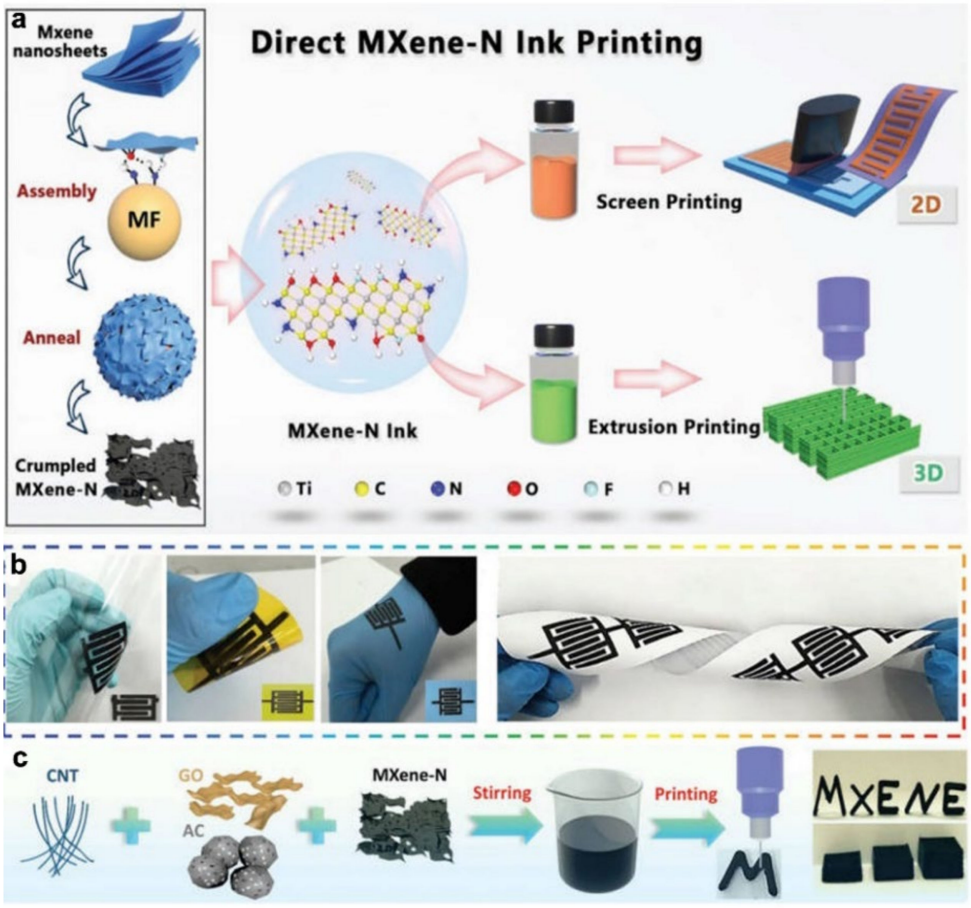

Figure 9. (**a**) Schematic illustration of the synthetic procedure for the crumpled MXene-N and the direct MXene-N ink printing routes of screen printing and extrusion printing. (**b**) Digital photographs of the MSC printed by screen printing. (**c**) Schematic showing of the preparation process of MXene-N based hybrid ink and the extrusion printed 3D architecture [56].

Zhang and co-workers employ the MXene sediments (usually thrown away) of unetched or multilayered MXene to prepare the additive free inks for scalable high-resolution screen printing. By designing different modes, various printed patterns (e.g., conductive tracks, letters, MSCs, and integrated circuits) can be quickly printed by using the as-formulated ink (Figure 10). They found that a low proportion of delaminated MXene flakes in the ink is crucial for realizing a desirable conductivity and excellent mechanical flexibility of the final printed circuitries or the electrodes. They also demonstrated an excellent electrochemical performance of the as-obtained printed MSCs with a high areal capacitance of 158 mF cm^{-2} and a high energy density of 1.64 μWh cm^{-2}. This ink formulation strategy of using MXene etching trash would effectively reduce the cost and waste of MXene-based printed techniques into consideration [83].

Liang et al. developed a thixotropic electrode ink that consisted of RuO_2-decorated $Ti_3C_2T_x$ MXene nanosheets ($RuO_2 \cdot xH_2O$@MXene) and conductive silver nanowires to fabricate the flexible printable MSC via the screen-printing method (Figure 11). They also found that the in situ growth of RuO_2 nanoparticles effectively relieves the agglomeration and restacking problems of the MXene flakes while maintains a suitable rheological nature for printing. Due to the synergistically interplayed effect of ingredients, the as-designed MSCs possess micrometer-scale resolution and desirable electrochemical properties, including a high volumetric capacitance of 864.2 F cm^{-3}, satisfactory energy/power densities of 13.5 mWh cm^{-3}/48.5 W cm^{-3}, a long-term cycling life with a retention of 90% after 10,000 cycles, and high mechanical stability [64].

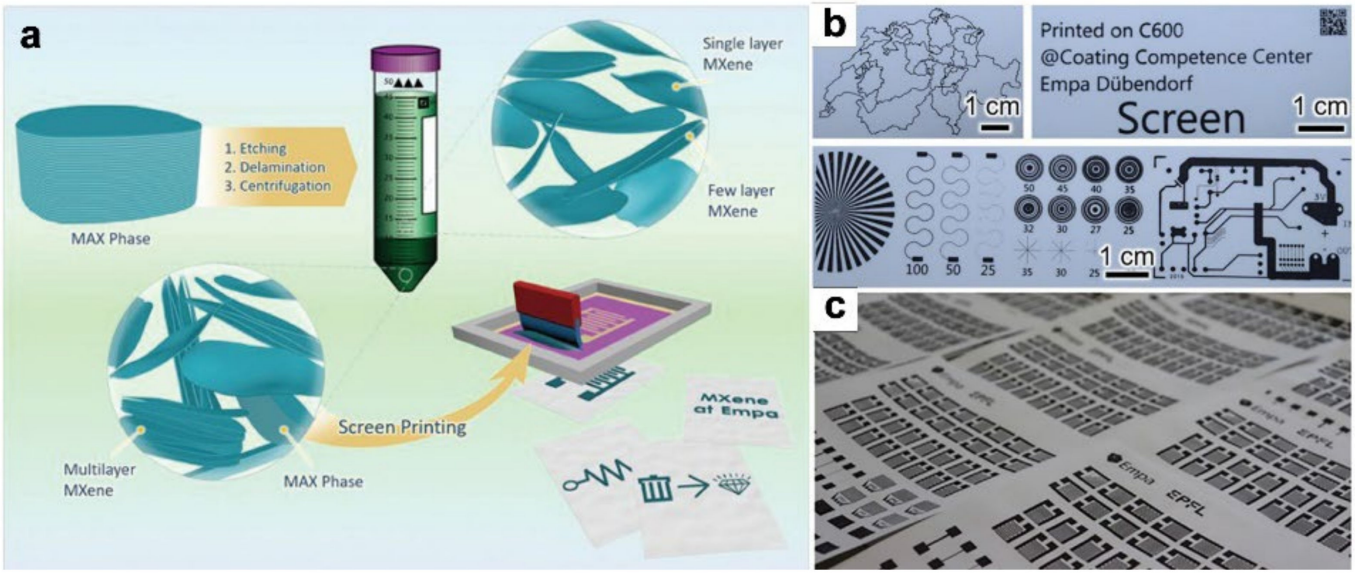

Figure 10. (**a**) Schematic illustrating of the screen printing using the MXene sediment ink. (**b**) Various screen-printed patterns. (**c**) Optical photo of scalable produced screen-printed MXene-based MSC [83].

The traditional micro-fabrication technologies that are based on the conventional silicon-based strategies, such as laser scribing, have also demonstrated feasibility for the fabrication of MXene-based MSC devices. For example, Hua's group employed the laser printing techniques with the assistance of vacuum deposition and physical sputtering to fabricate the MXene-based coplanar interdigital electrodes and planar symmetric on-chip MSC. They also reported that the as-developed fabrication method allows the deposition of fully delaminated MXene sheets with tunable thickness. Due to the good alignment of the MXene flakes, high electrical conductivity, and the unique layered porous structure of the as-designed MXene-based coplanar electrodes, the as-designed all-solid-state MSC displays excellent high-rate capacity, a high areal capacitance of 27.29 mF cm^{-2} and competitive volumetric energy densities of (5.48–6.1 mW h cm^{-3}) [84]. This work also demonstrated that

the MXene active materials have great potential for the laser printing process technology for patterning thick coplanar interdigital electrodes or planar SC.

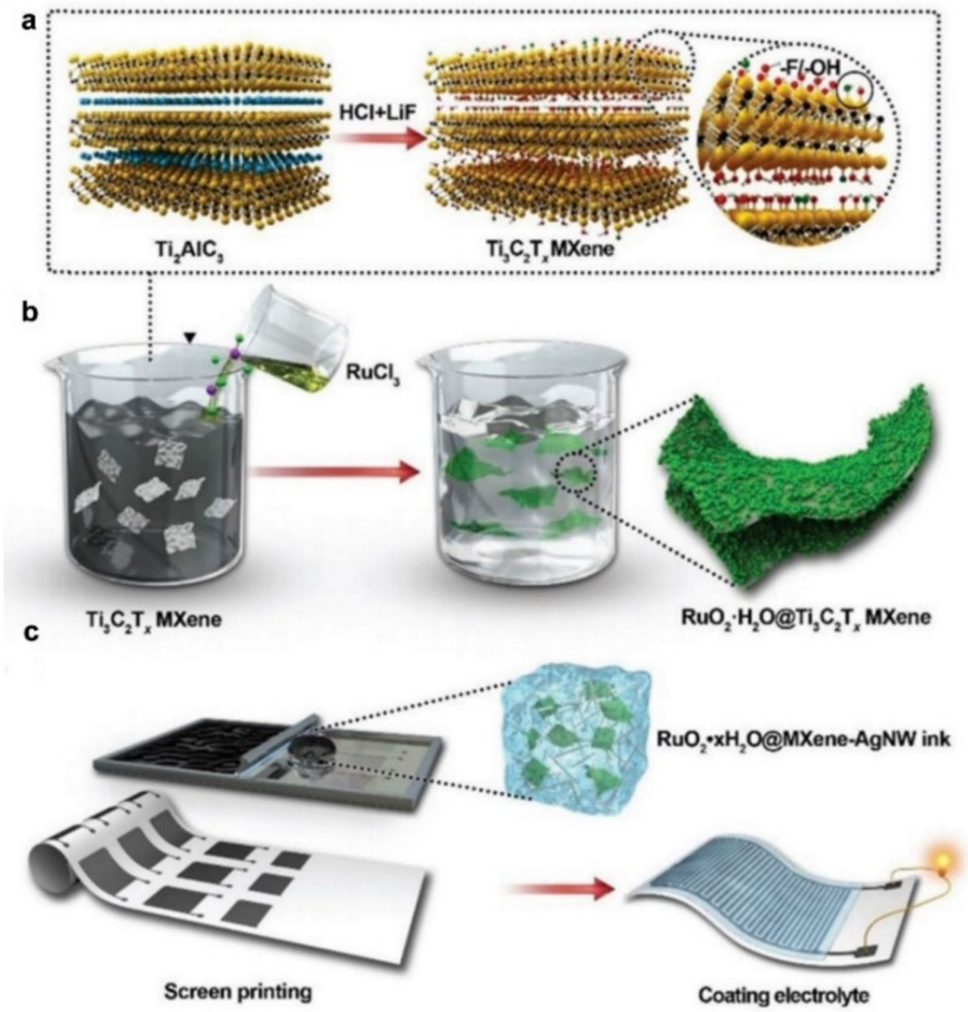

Figure 11. Schematic illustrating of (**a**) the preparation of MXene, (**b**) the synthesis process of the $RuO_2{\cdot}xH_2O$@MXene nanohybrid, and (**c**) the screen-printing process for the fabrication of the flexible MXene-based MSCs [64].

Flexible MXene-based yarn or fiber electrodes. Fiber-shaped SCs are attractive for powering miniaturized or portable wearable electronics due to their compatibility of integrating with textiles. In general, effective and scalable strategies to produce fiber electrodes with desirable electrical storage performances fall within two categories. The first category of deposition technique is based on covering of electrochemical active or conductive materials onto fiber matrix [85]. For instance, Yang and co-workers employed the MXene-polymer nanofibers as the coating layer on the polyester (PET) yarns to construct the PET@MXene nanofiber-based yarn via a modified electrospinning technique, from which the complex yarns display favorable flexibility and certain mechanical strength during the weaving, braiding, or knitting processes, indicating that the obtained yarns can be used as flexible yarn electrodes for wearable SCs. They also reported that two parallel PET@MXene yarn based SC devices delivered an areal capacitance of 18.39 mF cm^{-2} with desirable energy/power densities of 0.38 μWh cm^{-2}/0.39 mW cm^{-2} and long term stability (a retention percentage of 98.2% after 6000 cycles) [86].

Another fabrication approach for fiber production is wet-spinning method, which is more viable for industrial manufacture and applications [85]. Holistically, when con-

sidering the "spinnablility" for this approach to construct long continuous fibers, the high conductivity and available electrochemical activity provided by the composite formulations are the critical barrier hindering the electrochemical performances of the fiber electrodes. In addition, the homogeneous dispersion and the suitable spinning behaviors of the composite formulations also have an impact on the ultimate fiber properties (e.g., durability, flexibility, resilient stretching, bending, and twisting). In view of the hydrophilic properties and the excellent conductivity of MXene, which are suitable for wet-spinning processing, Seyedin and co-workers adopted the MXene ($Ti_3C_2T_x$) and poly(3,4-ethylenedioxythiophene):polystyrene sulfonate (PEDOT:PSS) to successfully fabricate an MXene/PEDOT:PSS hybrid fiber electrode. By combining with the flexible PEDOT:PSS, the as-designed optimized $Ti_3C_2T_x$-based fiber electrode (containing 70% MXene and 30% PEDOT:PSS, referred to as M_7P_3) exhibited a record conductivity of 1.489 S cm^{-1}, a high volumetric capacitance of 614.5 F cm^{-3} at 5 mV s^{-1}, and an excellent rate performance of 375.2 F cm^{-3} at 1000 mV s^{-1} in a potential range of −0.8–0.2 V with a three-electrode setup in 1 M H_2SO_4 electrolyte. The as-designed fiber SC device in an operated voltage of 0.6 V could deliver maximum volumetric energy/power densities of 7.13 Wh cm^{-3}/8.249 mW cm^{-3}. Moreover, a stretchable and elastic fiber SC prototype assembled by prestretched silicon rubber and M_7P_3 wrapping with a PVA/H_2SO_4 electrolyte maintains capacitance retention of ≈98% and ≈96% after cyclically stretched under different stretched strains [85].

Flexible stretchability MXene-based electrodes. The unique properties of MXene (e.g., metallic conductivity, strong interactions among large flakes, hydrophilic surface groups, and high volumetric capacitance (up to 1500 F cm^{-3})) enable them particularly attractive for stretchable energy storage devices or electronics. Nevertheless, the fragility and high mechanical modulus (3–75 GPa) at dry state for MXene would increase the device resistance when subjected to larger tensile strains and further limit their stable electrochemical outputs [30]. To address these challenges and constraints, several methods have been developed for constructing robust SC electrodes with high stretchability, superior electrochemical performance, and high chemical stability. Chen and co-workers used a sequential patterning approach to prepare high dimensional MXene nanocoatings with mechanically stable architectures, which can be program crumpling and unfolding. After transferring on the elastomer, MXene/elastomer SC electrodes were obtained, which show high stretchability for reversibly folded/unfolded. A stretchable asymmetric SC fabricated by using the as-obtained electrodes is capable of delivering stable electrochemical output under various mechanical deformations (e.g., bend or stretch), such as favorable capacitances of 395, 390, and 362 F cm^{-3} under 0%, 50%, and 80% strains, efficient energy density of 5.5 Wh kg^{-1}, and long term cycling stability under stretching/bending conditions [87].

Some works also revealed that the combination of $Ti_3C_2T_x$ with other high mechanical robustness nanomaterials (e.g., reduced graphene oxide (RGO)) would generate flexible and stretchable free-standing electrodes with superior electrochemical performance. Cao and co-workers adopted the MXene ($Ti_3C_2T_x$ in this case) and RGO to fabricate a robust and stretchable electrode ($Ti_3C_2T_x$/RGO composite) for flexible SC devices. The test results show that the final composite with 50 wt% RGO would alleviate cracks that result from large strains. Due to strong nanosheet interactions between larger nanoflakes, mechanical flexibility, and excellent electrochemical properties of each component, the as-obtained electrode delivered a capacitance of 49 mF cm^{-2} (~490 F cm^{-3} and ~140 F g^{-1}) with high mechanical stability after various cyclic strains (e.g., uniaxial and biaxial strains). An all-solid-state stretchable symmetric SC fabricated by these electrodes displayed a high capacitance of 18.6 mF cm^{-2} (~90 F cm^{-3} and ~29 F g^{-1}) with high mechanical stretchability [30,87–90]. The comparison of the electrochemical performance of various MXene-based materials for SCs are listed in Table 1.

Table 1. Comparison of the electrochemical properties of different MXene-based materials for SCs.

Materials	Capacity/Current Density	Capacity Retention	Energy Density and Power Density	Reference
1T-MoS_2/Ti_3C_2MXene based flexible ASSS	386.7 F g^{-1} at 1 A g^{-1}	91.1% after 20,000 cycles at 30 mA cm^{-2}	17.4 μW h cm^{-2} (600 μW cm^{-2})	[66]
TC-9//Ti_3C_2 ASC	49.3 F g^{-1} at 1 A g^{-1}	82.4% after 5000 cycles at 8 A g^{-1}	15.4 W h kg^{-1} (750.2 W kg^{-1})	[65]
MXene/LDH composite	1061 F g^{-1} at 1 A g^{-1}	70% after 4000 cycles at 4 A g^{-1}		[67]
M-$Ti_3C_2T_x$//PANI	510 F g^{-1} at 10 mV s^{-1}		50.6 W h L^{-1} (1.7 kW L^{-1})	[73]
N-$Ti_3C_2T_x$-200 °C	192 F g^{-1} at 1 mV s^{-1}	92% after 10,000 cycles at of 50 mV s^{-1}	8.07 W h kg^{-1} (52.8 W kg^{-1})	[69]
all-solid-state symmetric SCs based on MXene/MPFs electrode	408 mF cm^{-2} at 0.5 mA cm^{-2}	95.9% after 7000 cycles at 5 mA cm^{-2}	20.4 μW h cm^{-2} (152.2 μW cm^{-2})	[75]
all-solid-state SC based on PDT/$Ti_3C_2T_x$	52.4 mF cm^{-2} (3.52 F cm^{-3}) at 0.1 mA cm^{-2}		24 mW h cm^{-3} (502 mW cm^{-3})	[76]
FSC based on FQDs/CNTC film	71.26 F cm^{-3} at 10 mV s^{-1}	80% after 10,000 cycles at 4 A cm^{-3}	77.12 mW h cm^{-3} (750 mW cm^{-3})	[78]
$Ti_3C_2T_x$/CNF MSC	25.3 mF cm^{-2} at 2 mV s^{-1}	86.8% after 10,000 cycles at 0.57 mA cm^{-2}	0.08 μWh cm^{-2} (145 μW cm^{-2})	[79]
PANI//$Ti_3C_2T_x$ device	925 mF cm^{-2} (87 F g^{-1}) at 3 mA cm^{-2}	93% after 10,000 cycles at 50 mA cm^{-2}	252 μW h cm^{-2} (2.12 mW cm^{-2})	[80]
M/MoO_3 symmetric SC	396 F cm^{-3} (118.8 F g^{-1}) at mV s^{-1}	90% after 5000 cycles at 30 mA cm^{-2}	13.4 W h kg^{-1} (534.6 W kg^{-1})	[82]
MXene NCY SC	18.39 mF cm^{-2} at 5 mV s^{-1}	98.2% after 6000 cycles at 50 mV s^{-1}	0.38 μW h cm^{-2} (0.39 mW cm^{-2})	[86]
MXene-N MSC	70.1 mF cm^{-2} at 10 mV s^{-1}	92% after 7000 cycles at 5 mA cm^{-2}	0.42 mW h cm^{-2} 0.83 mW h cm^{-3}	[56]
MSCs based on this RuO_2·xH_2O@MXene–AgNW nanocomposite ink	864.2 F cm^{-3} at 1 mV s^{-1}	90% after 10,000 cycles at 100 mV s^{-1}	13.5 mW h cm^{-3} (1.1 W cm^{-3})	[64]

3.2. Li Ions Battery (LIB)

MXenes also display great potential in LIB due to their large available surface areas for electrolyte ion adsorption, satisfactory electrical conductivity, desirable ion transfer within the inter-layers (up to 1.3 nm), and rapid surface redox reaction. Additionally, the MXenes (e.g., Ti_3C_2) can also be used as functional host matrix for integrating other materials for further enhancing the overall energy storage performance of LIB [91]. For instance, Junjie Niu's group synthesized a hybrid material comprising Ti_3C_2 MXene wrapped with germanium oxide layer (GeO_x (x = 1.57) @MXene) through the wet-chemical strategy. The high electronic conductivity of MXene and germanium enable a high rate capability, superb capacity retention of ~929.6 mAh g^{-1} at 1.0 C with high Coulombic efficiency of 99.6% after 1000 cycle. Especially, the as-designed LIB also possesses temperature dependence properties [91]. Likun Pan's group prepared a SnS_2/Sn_3S_4 modified multi-layered Ti_3C_2 MXene hybrid (denoted as S-TC) as anode material for LIB via the solvothermal and calcination strategy. The MXene substrate provides high electronic conductivity and suppresses the aggregation and volume change problems of active components while the nano-sized SnS_2/Sn_3S_4 acts as a "spacer" to effectively inhibit restacking of the Ti_3C_2 layer. Due to these reasons, the S-TC anode delivers superb rate capability (216.5 mAh g^{-1} at 5 A g^{-1}) coupled with long cycling stability [92]. Wang et al. rationally designed an interconnected MXene hybrid aerogel composited with Fe_2O_3 nanospheres, which exhibits superb energy density of 216 Wh kg^{-1} at 400 W kg^{-1} for lithium-ion capacitors due to the synergistic effect between the two components [93]. Husam N. Alshareef et al. synthesized a HfO_2 coated SnO_2/MXene composite anode material via atomic layer deposition. The deposited SnO_2 on the MXene can effectively suppress the degradation of MXene while the thin inactive layer of HfO_2 would serve as an artificial solid-electrolyte

interphase (SEI) layer for further enhancing the cycling stability [94]. Wang et al. found that the integrating of nitrogen and vanadium in the forms of C–V–OH, C–V–O, V–O, and Ti–O–N species into the Ti-deficient $Ti_3C_2T_x$ can further enhance the charge storage capability for approximately 40% [95]. Wang and co-workers modulated the interfacial properties by fabricating a crumpled S-functionalized $Ti_3C_2T_x$ heterostructure embedded with Fe_3O_4/FeS. Due to the tuned electronic properties, the heterostructure displays improved kinetics and structural stability for LIB. The authors claimed that the S terminations boosted the extra (pseudo)capacitive ability of MXene for lithium storage. Due to these reasons, the optimized anode of the heterostructure material delivers a superb long-term stability (913.9 mAh g^{-1} after 1000 cycles) with desirable rate performance. They also found that the heterostructure material exhibits an asymmetric conversion mechanism by experiencing stepwise phase transformations under discharge process coupled with a relatively uniform reconversion under the charge process. This work gives an in-depth understanding about MXene-based heterostructure for Li ion storage [96].

Yan and co-workers improved the properties of MXene by employing a liquid nitrogen quenching method to roll up the MXene sheets into $Ti_3C_2T_x$ scrolls. They found that the prepared scrolls display unclosed topological structure and can effectively relieve the restacking effect. Meanwhile, they also reported that the produced scrolls possess superior electrical conductivity and can be used as buffer matrixes of Si nanoparticles for electrochemical energy storage. Due to these reasons, the as-designed $Ti_3C_2T_x$ scroll anode material exhibits a reversible capacity of 226 mAh g^{-1}, desirable rate performance, and excellent long-term cycling performance with 81.6% capacity retention after 500 cycles in LIB.

Additionally, MXene materials can be directly used as conductive and highly stable hosts by forming artificial solid electrolyte interface (SEI) film for greatly reducing the topical current density on the surface of the electrode, adjusting the electric field, and efficiently inducing the uniform growth of lithium dendrites. As exemplified, Shubin Yang's group demonstrated that the parallelly aligned MXene layers (denoted as PA-MXene-Li) can effectively regulate the uniform nucleation and growth of lithium, forming horizontal-growth of lithium on the surface of MXene. Moreover, the fluorine terminations of MXene make forming a durable and artificial solid electrolyte interface with lithium fluoride and homogenizing the electro-migration for lithium ions during the energy storage process possible [97].

Flexible MXene thin films or free-standing electrodes. The diversification development of LIBs (portable, flexible, wearable, stretchable, and foldable, etc.) is urgently required for ever-increasing demands for future energy-storage devices. In this respect, exploring conductive and flexible substrate with strong coupling of active materials is the key factor for the application of flexible LIBs technology. Given the self-assembly ability, 2D MXene are considered as ideal matrix to load active materials for forming composite paper electrodes in flexible LIBs. For example, Yitai Qian's group developed a MXene/liquid metal paper by confining the low-melting point GaInSnZn liquid metal in the MXene substrate. Due to the excellent conductivity and satisfactory wettability between GaInSnZn and MXene matrix, the obtained flexible anode for LIB exhibits a higher capacity of 638.79 mAh g^{-1} at 20 mA g^{-1} coupled with desirable rate performance (which is better than that of liquid metal coated Cu foil), indicating that the great potential of MXene matrix for compositing with various active materials in flexible LIB [98]. Feng et al. demonstrated that the construction of the Silicon/MXene composite papers via vacuum filtration to covalently anchor silicon nanospheres on MXene can accommodate the volumetric expansion of silicon and restrain the restacking of MXene sheets, which offers superior capacity of 2,118 mAh·g^{-1} at a current density of 200 mA·g^{-1} [18]. The electrochemical performances of different MXene-based materials for LIBs are compared and listed in Table 2.

Table 2. Comparison of the electrochemical properties of different MXene-based materials for LIBs.

Materials	Capacity/Current Density	Cycling Stability	Rate Capacity	Reference
GeO_2@MXene	1127.1 mA h g^{-1} at 0.5 C	1048.1 mA h g^{-1} at 0.5 C after 500 cycles	221.2 mAh g^{-1} at 20.0 C	[91]
S-TC	601.3 mA h g^{-1} at 100 mA g^{-1}	426.3 mA h g^{-1} at 100 mA g^{-1} after 100 cycles	216.5 mAh g^{-1} at 5000 mA g^{-1}	[92]
N(V)-modified $Ti_3C_2T_x$MXene	251.3 mA h g^{-1} at 0.1 C	92 mA h g^{-1} at 3C after 1000 cycles	118.3 mA h g^{-1} at 5 C	[95]
Fe_3O_4/FeS 30@S-MX	746.6 mAh g^{-1} at 0.1 A g^{-1}	913.9 mA h g^{-1} after 1000 cycles at 1 A g^{-1}	490.4 mA h g^{-1} at 10 A g^{-1}	[96]

3.3. Zn Ions Storage Devices

Recent works suggest that the MXene can also be used as both anode and cathode materials for zinc ion hybrid supercapacitors (ZHSCs). As Qi Yang and co-workers demonstrated, the Zn−MXene capacitor fabricated by Ti_3C_2 cathode and the Zn@Ti_3C_2 anode displays 82.5% capacitance retention after 1000 cycles with excellent anti-self-discharge ability of 6.4 mV h^{-1} [99]. The MXene ($Ti_3C_2T_x$) is directly used as anode coupled with manganese dioxide/carbon nanotubes (MnO_2-CNTs) cathode material to fabricate a zinc-ion capacitor (ZIC). The obtained ZIC in aqueous electrolyte possesses a high specific capacitance, energy density of 98.6 Wh kg^{-1}, and high capacitance retention of ~83.6% after 15,000 cycles [100]. Wang et al. reported that when the δ-MnO_2 cathode and MXene are grown on the cotton cloth, the assembled device would exhibit a high energy density of 90 Wh kg^{-1} with capacitance retention of ~80.7% after 16,000 cycles [101]. Others would like to employ the MXene as a protective layer for suppressing the growth of Zn dendrites. Qian's group investigated the growth mechanism of metal zinc on the surface of Zn foil and binder-free $Ti_3C_2T_x$ MXene@Zn hybrid firm and found that the $Ti_3C_2T_x$ MXene@Zn film effectively restrains the growth of Zn dendrites with reversible plating/stripping of Zn. The developed MXene film would be a valid strategy for dendrite-free electrochemical storage devices [3]. Zeng et al. adopted the MXene with the reduced graphene oxide (rGO) to fabricate a 3D porous MXene-rGO aerogel for preventing the restacking of MXene flakes and enhancing the electrical conductivity and hydrophilicity of the final materials. The electrochemical results show that the ZHSC with the MXene-rGO aerogel cathode delivers a high specific capacitance of 128.6 F g^{-1} coupled with high energy density of 34.9 Wh kg^{-1} and long term stability for 75,000 cycles [2]. The comparison of the electrochemical performance of various MXene-based materials for Zn ions storage devices are listed in Table 3.

Table 3. Comparison of the electrochemical properties of different MXene-based materials for Zn ions storage devices.

Materials	Capacity/Current Density	Cycling Stability	Energy Density and Power Density	Reference
Zn@Ti_3C_2 anode and Ti_3C_2 film cathode	132 F g^{-1} at 0.5 A g^{-1}	82.5% after 1000 cycles at 3 A g^{-1}		[99]
MnO_2–CNTs cathode and MXene anode	115.1 F g^{-1} at 1 mV s^{-1}	83.6% at 15,000 cycles at 5.224 A g^{-1}	98.6 W h kg^{-1} (77.5 W kg^{-1})	[100]
MXene-rGO2//$ZnSO_4$//Zn	128.6 F g^{-1} at 0.4 A g^{-1}	95% after 75,000 cycles at 5 A g^{-1}	34.9 W h kg^{-1} (279.9 W kg^{-1})	[2]

4. Conclusions

In summary, this review was mainly focused on the synthetic method, the construction of MXene hybrids, and composite films or fibers in terms of their performance for various energy storage devices. The most recent advances of technologies (e.g., vacuum filtration, extrusion printing technique, and directly writing) for fabricating patterned MXene-based composite films or fibers with geometric flexibility in various energy storage devices were described. The multifunctional properties of MXenes enable them to be used as electrodes for SCs and anode materials for both lithium- and zinc-ion batteries. As we introduced

above, the electrochemical performance of MXene-based materials can be enhanced by tuning the chemical components, constructing the micro/nano structures, and enlarging the interlayer of MXene flakes. Advanced MXene-based macroscopically assembled films and fibers with dedicated design were also demonstrated in this work, which are expected to significantly enhance the geometric flexibility for portable energy storage devices. Thus, it is expected that the MXene-based nanostructures and advanced architectures for films and fibers will provide intriguing opportunities for next generation energy storage devices.

1. MXene offers attractive properties in SC applications, such as excellent conductivity, ultrahigh rate capability, adjustable composition, hydrophilic, and volumetric capacitance. Still, the stacking and aggregating problems reduce the interlayer spaces and lead to the sluggish kinetics for energy storage. Therefore, many MXene-based composites (e.g., 2D/2D 1T-MoS_2/Ti_3C_2 heterostructures, Ti_3C_2/CuS, MXene/LDH, Ni–S/Ti_3C_2 nanohybrid, N-doped MXene, N, O co-doped carbon@MXene composite, dodecaborate/MXene) were designed for solving the problems via the surface modification, heteroatom doping, or crumpling process. Among the various materials, the Ni–S/Ti_3C_2 composite exhibits a superior capacity of 840.4 C g^{-1} with a retention of 64.3% at 30 A g^{-1} and a long cycle life. In addition, in order to settle the easy oxidation issue at positive potential (anodic oxidation process) of MXenes and most MXene-derived composites, some works focus on the enhancing of the WF to boost the antioxidant ability of MXene-based materials. PANI@MXene cathode material exhibits a larger WF due to the existence of the oxidation-resistive PANI layer on the surface of MXene compared with the pure metallic MXene, which enhance the electrochemical stability at a wider positive operating potential (0–0.6 V).

2. The special flexibility and self-assembly capability of MXenes enable them to be a versatile unit for constructing the macroscopic film and fiber electrodes. Several assembly strategies are developed, including spin-casting method, vacuum-assisted filtration method, and electrophoretic deposition/spin coating coupled method. Additionally, the energy storage performance can be further enhanced by optimizing the MXene synthesis conditions, tuning the MXene interlayer spacing, altering the types or amount of surface terminations, and compositing with other functional materials. Many recent works also revealed that the addition of reinforcement (e.g., carboxymethylated cellulose nanofibrils, bacterial cellulose) also acts as spacers for MXene to fabricate robust film electrodes with strong mechanical strength.

3. MXenes can be employed as the printing material for constructing the geometric flexible, printable, and free-standing electrochemical devices (e.g., MXene-based coplanar interdigital electrodes, printable or direct-write SC devices) due to their hydrophilicity, mechanical flexibility, and modifiability. In this regard, the design of certain formulations of MXene-based conductive inks with specific rheological properties for the compatibility with various patterning methods (e.g., screen printing, direct writing, and extrusion printing) was crucial for the fabrication of the printable energy storage devices.

4. MXenes can also be used for LIBs and Zn ions storage devices due to their layer structure for electrolyte ion adsorption, satisfactory electrical conductivity, and desirable ion transfer ability within the layers. Many recent works reveal that the compositing with other functional materials can further enhance the overall energy storage performance (e.g., GeO_x (x = 1.57)@MXene, SnS_2/Sn_3S_4 modified multi-layered Ti_3C_2 MXene hybrid, SnO_2/MXene composite, MXene/liquid metal, silicon/MXene, and MXene-rGO aerogel). Among the various materials, the GeO_x (x = 1.57)@MXene exhibits a high rate capability, superb capacity retention of ~929.6 mAh g^{-1} at 1.0 C with high Coulombic efficiency of 99.6% after 1000 cycles.

With further substantial research effort on optimized methodologies, MXenes and their derivatives represent a promising platform in scalable and customizable manufacturing of multipurpose electrodes with wearable, flexible, and lightweight properties in the future.

Author Contributions: Conceptualization, H.M. and S.Y.; investigation, C.J. and H.C.; data curation, H.C.; writing—original draft preparation, C.J. and H.C.; writing—review and editing, C.J. and H.C.; visualization, H.C.; supervision, S.Y.; project administration, S.Y.; funding acquisition, S.Y. and C.J. All authors have read and agreed to the published version of the manuscript.

Funding: This research was funded by the National Natural Science Foundation of China, grant number 21805237, U2003132. Fundamental Research Funds for the Central Universities and the Natural Science Foundation of Shaanxi Province, grant number 2021GXLH-Z-082 and 2020JZ-02 (S. Yang). Natural Science Foundation of Xinjiang Uygur Autonomous Region, grant number 2018D01C053. Tianshan Youth Planning Program of Science & Technology Department of Xinjiang Uygur Autonomous Region, grant number 2018Q013. Opening Foundation of the State Key Laboratory of Fine Chemicals, grant number KF2003.

Institutional Review Board Statement: Not applicable.

Informed Consent Statement: Not applicable.

Data Availability Statement: No data support.

Conflicts of Interest: The authors declare no conflict of interest.

References

1. Jakob, M.; Hilaire, J. Unburnable fossil-fuel reserves. *Nature* **2014**, *517*, 150–151. [CrossRef]
2. Wang, Q.; Wang, S.; Guo, X.; Ruan, L.; Wei, N.; Ma, Y.; Li, J.; Wang, M.; Li, W.; Zeng, W. MXene-reduced graphene oxide aerogel for aqueous zinc-ion hybrid supercapacitor with ultralong cycle life. *Adv. Electron. Mater.* **2019**, *5*, 1900537. [CrossRef]
3. Tian, Y.; An, Y.; Wei, C.; Xi, B.; Xiong, S.; Feng, J.; Qian, Y. Flexible and free-standing $Ti_3C_2T_x$ MXene@Zn paper for dendrite-free aqueous zinc metal batteries and nonaqueous lithium metal batteries. *ACS Nano* **2019**, *13*, 11676–11685. [CrossRef] [PubMed]
4. Herou, S.; Bailey, J.J.; Kok, M.; Schlee, P.; Jervis, R.; Brett, D.J.L.; Shearing, P.R.; Ribadeneyra, M.C.; Titirici, M. High-density lignin-derived carbon nanofiber supercapacitors with enhanced volumetric energy density. *Adv. Sci.* **2021**, *8*, 2100016. [CrossRef]
5. Ma, X.; Cheng, J.; Dong, L.; Liu, W.; Mou, J.; Zhao, L.; Wang, J.; Ren, D.; Wu, J.; Xu, C.; et al. Multivalent ion storage towards high-performance aqueous zinc-ion hybrid supercapacitors. *Energy Storage Mater.* **2019**, *20*, 335–342. [CrossRef]
6. Rojaee, R.; Shahbazian-Yassar, R. Two-dimensional materials to address the lithium battery challenges. *ACS Nano* **2020**, *14*, 2628–2658. [CrossRef] [PubMed]
7. Mao, J.; Zhou, T.; Zheng, Y.; Gao, H.; Liua, H.K.; Guo, Z. Two-dimensional nanostructures for sodium-ion battery anodes. *J. Mater. Chem. A* **2018**, *6*, 3284–3303. [CrossRef]
8. Lin, L.; Lei, W.; Zhang, S.Y.; Liu, G.G.; Wallace, J.C. Two-dimensional transition metal dichalcogenides in supercapacitors and secondary batteries. *Energy Storage Mater.* **2019**, *19*, 408–423. [CrossRef]
9. Zhu, H.; Zhang, F.; Li, J.; Tang, Y. Penne-like MoS_2/carbon nanocomposite as anode for sodium-ion-based dual-ion battery. *Small* **2018**, *14*, 1703951. [CrossRef] [PubMed]
10. Haseeb, H.H.; Li, Y.; Ayub, S.; Fang, Q.; Yu, L.; Xu, K.; Ma, F. Defective phosphorene as a promising anchoring material for lithium–sulfur batteries. *J. Phys. Chem. C* **2020**, *124*, 2739–2746. [CrossRef]
11. Leng, K.; Li, G.; Guo, J.; Zhang, X.; Wang, A.; Liu, X.; Luo, J. A safe polyzwitterionic hydrogel electrolyte for long-life quasi-solid state zinc metal batteries. *Adv. Funct. Mater.* **2020**, *30*, 2001317. [CrossRef]
12. Zhang, H.; Liu, Q.; Fang, Y.; Teng, C.; Liu, X.; Fang, P.; Tong, Y.; Lu, X. Boosting Zn-ion energy storage capability of hierarchically porous carbon by promoting chemical adsorption. *Adv. Mater.* **2019**, *31*, 1904948. [CrossRef]
13. Xiao, Z.; Li, Z.; Meng, X.; Wang, R. MXene-engineered lithium-sulfur batteries. *J. Mater. Chem. A* **2019**, *7*, 22730–22743. [CrossRef]
14. Zhang, X.; Zhang, Z.; Zhou, Z. MXene-based materials for electrochemical energy storage. *J. Energy Chem.* **2018**, *27*, 73–85. [CrossRef]
15. Lei, J.C.; Zhang, X.; Zhou, Z. Recent advances in MXene: Preparation, properties, and applications. *Front. Phys.* **2015**, *10*, 276–286. [CrossRef]
16. Jiang, Q.; Lei, Y.; Liang, H.; Xi, K.; Xia, C.; Alshareef, H.N. Review of MXene electrochemical microsupercapacitors. *Energy Storage Mater.* **2020**, *27*, 78–95. [CrossRef]
17. Zhao, Q.; Zhu, Q.; Liu, Y.; Xu, B. Status and prospects of MXene-based lithium–sulfur batteries. *Adv. Funct. Mater.* **2021**, *31*, 2100457. [CrossRef]
18. Tian, Y.; An, Y.; Feng, J. Flexible and freestanding silicon/MXene composite papers for high-performance lithium-ion batteries. *ACS Appl. Mater. Interfaces* **2019**, *11*, 10004–10011. [CrossRef] [PubMed]
19. Wang, H.; Wu, Y.; Yuan, X.; Zeng, G.; Zhou, J.; Wang, X.; Chew, J.W. Clay-inspired MXene-based electrochemical devices and photo-electrocatalyst: State-of-the-art progresses and challenges. *Adv. Mater.* **2018**, *30*, 1704561. [CrossRef] [PubMed]
20. Yu, H.; Wang, Y.; Jing, Y.; Ma, J.; Du, C.F.; Yan, Q. Surface modified MXene-based nanocomposites for electrochemical energy conversion and storage. *Small* **2019**, *15*, 1901503. [CrossRef]
21. Gogotsi, Y.; Anasori, B. The rise of MXenes. *ACS Nano* **2019**, *13*, 8491–8494. [CrossRef]

22. Yang, Q.; Xu, Z.; Fang, B.; Huang, T.; Cai, S.; Chen, H.; Liu, Y.; Gopalsamy, K.; Gao, W.; Gao, C. MXene/graphene hybrid fibers for high performance flexible supercapacitors. *J. Mater. Chem. A* **2017**, *5*, 22113–22119. [CrossRef]
23. Li, X.; Ma, Y.; Shen, P.; Zhang, C.; Yan, J.; Xia, Y.; Luo, S.; Gao, Y. Self-healing microsupercapacitors with size-dependent 2D MXene. *ChemElectroChem* **2020**, *7*, 821–829. [CrossRef]
24. Liu, J.; Zhang, H.B.; Sun, R.; Liu, Y.; Liu, Z.; Zhou, A.; Yu, Z.Z. Hydrophobic, flexible, and lightweight MXene foams for high-performance electromagnetic-interference shielding. *Adv. Mater.* **2017**, *29*, 1702367. [CrossRef] [PubMed]
25. Zha, X.-H.; Zhou, J.; Zhou, Y.; Huang, Q.; He, J.; Francisco, J.S.; Luoa, K.; Du, S. Promising electron mobility and high thermal conductivity in Sc_2CT_2 (T = F, OH) MXenes. *Nanoscale* **2016**, *8*, 6110–6117. [CrossRef]
26. Xu, N.; Li, H.; Gan, Y.; Chen, H.; Li, W.; Zhang, F.; Jiang, X.; Shi, Y.; Liu, J.; Wen, Q.; et al. Zero-dimensional MXene-based optical devices for ultrafast and ultranarrow photonics applications. *Adv. Sci.* **2020**, *7*, 2002209. [CrossRef]
27. Wu, Y.; Hu, H.; Yuan, C.; Song, J.; Wu, M. Electrons/ions dual transport channels design: Concurrently tuning interlayer conductivity and space within re-stacked few-layered MXenes film electrodes for high-areal-capacitance stretchable micro-supercapacitor-arrays. *Nano Energy* **2020**, *74*, 104812. [CrossRef]
28. Pan, Z.; Ji, X. Facile synthesis of nitrogen and oxygen co-doped C@Ti_3C_2 MXene for high performance symmetric supercapacitors. *J. Power Source* **2019**, *439*, 227068. [CrossRef]
29. Li, M.; Li, X.; Qin, G.; Luo, K.; Lu, J.; Li, Y.; Liang, G.; Huang, Z.; Zhou, J.; Hultman, L.; et al. Halogenated Ti_3C_2 MXenes with electrochemically active terminals for high-performance zinc ion batteries. *ACS Nano* **2021**, *15*, 1077–1085. [CrossRef]
30. Zhou, Y.; Maleski, K.; Anasori, B.; Thostenson, J.O.; Pang, Y.; Feng, Y.; Zeng, K.; Parker, C.B.; Zauscher, S.; Gogotsi, Y.; et al. $Ti_3C_2T_x$ MXene-reduced graphene oxide composite electrodes for stretchable supercapacitors. *ACS Nano* **2020**, *14*, 3576–3586. [CrossRef]
31. Lu, M.; Han, W.; Li, H.; Li, H.; Zhang, B.; Zhang, W.; Zheng, W. Magazine-bending-inspired architecting anti-T of MXene flakes with vertical ion transport for high-performance supercapacitors. *Adv. Mater. Interfaces* **2019**, *6*, 1900160. [CrossRef]
32. Meng, J.; Zhang, F.; Zhang, L.; Liu, L.; Chen, J.; Yang, B.; Yan, X. Rolling up MXene sheets into scrolls to promote their anode performance in lithium-ion batteries. *J. Energy Chem.* **2020**, *46*, 256–263. [CrossRef]
33. Shi, H.; Yue, M.; Zhang, C.J.; Dong, Y.; Lu, P.; Zheng, S.; Huang, H.; Chen, J.; Wen, P.; Xu, Z.; et al. 3D flexible, conductive, and recyclable $Ti_3C_2T_x$ MXene-melamine foam for high-areal-capacity and long-lifetime alkali-metal anode. *ACS Nano* **2020**, *14*, 8678–8688. [CrossRef]
34. Fan, Z.; Wei, C.; Yu, L.; Xia, Z.; Cai, J.; Tian, Z.; Zou, G.; Dou, S.X.; Sun, J. 3D printing of porous nitrogen-doped Ti_3C_2 MXene scaffolds for high-performance sodium-ion hybrid capacitors. *ACS Nano* **2020**, *14*, 867–876. [CrossRef]
35. Dong, Y.; Shi, H.; Wu, Z.S. Recent advances and promise of MXene-based nanostructures for high-performance metal ion batteries. *Adv. Funct. Mater.* **2020**, *30*, 2000706. [CrossRef]
36. Huang, H.; Jiang, R.; Feng, Y.; Ouyang, H.; Zhou, N.; Zhang, X.; Wei, Y. Recent development and prospects of surface modification and biomedical applications of MXenes. *Nanoscale* **2020**, *12*, 1325–1338. [CrossRef] [PubMed]
37. Pang, J.; Mendes, R.G.; Bachmatiuk, A.; Zhao, L.; Ta, H.Q.; Gemming, T.; Liu, H.; Liu, Z.; Rummeli, M.H. Applications of 2D MXenes in energy conversion and storage systems. *Chem. Soc. Rev.* **2019**, *48*, 72–133. [CrossRef]
38. Nan, J.; Guo, X.; Xiao, J.; Li, X.; Chen, W.; Wu, W.; Liu, H.; Wang, Y.; Wu, M.; Wang, G. Nanoengineering of 2D MXene-based materials for energy storage applications. *Small* **2021**, *17*, 1902085. [CrossRef] [PubMed]
39. Xiong, D.; Li, X.; Bai, Z.; Lu, S. Recent advances in layered $Ti_3C_2T_x$ MXene for electrochemical energy storage. *Small* **2018**, *14*, 1703419. [CrossRef] [PubMed]
40. Alhabeb, M.; Maleski, K.; Anasori, B.; Lelyukh, P.; Clark, L.; Sin, S.; Gogotsi, Y. Guidelines for synthesis and processing of two-dimensional titanium carbide ($Ti_3C_2T_x$ MXene). *Chem. Mater.* **2017**, *29*, 7633–7644. [CrossRef]
41. Barsoum, B.M.W. *MAX Phases: Properties of Machinable Ternary Carbides and Nitrides*; Wiley-VCH Verlag GmbH & Co. KGaA: Weinheim, Germany, 2013.
42. Naguib, M.; Kurtoglu, M.; Presser, V.; Lu, J.; Niu, J.; Heon, M.; Hultman, L.; Gogotsi, Y.; Barsoum, M.W. Two-dimensional nanocrystals produced by exfoliation of Ti_3AlC_2. *Adv. Mater.* **2011**, *23*, 4248–4253. [CrossRef] [PubMed]
43. Halim, J.; Lukatskaya, M.R.; Cook, K.M.; Lu, J.; Smith, C.R.; Naslund, L.A.; May, S.J.; Hultman, L.; Gogotsi, Y.; Eklund, P.; et al. Transparent conductive two-dimensional titanium carbide epitaxial thin films. *Chem. Mater.* **2014**, *26*, 2374–2381. [CrossRef] [PubMed]
44. Shahzad, F.; Alhabeb, M.; Hatter, C.B.; Anasori, B.; Hong, S.M.; Koo, C.M.; Gogotsi, Y. Electromagnetic interference shielding with 2D transition metal carbides (MXenes). *Science* **2016**, *353*, 1137–1140. [CrossRef] [PubMed]
45. Lipatov, A.; Alhabeb, M.; Lukatskaya, M.R.; Boson, A.; Gogotsi, Y.; Sinitskii, A. Effect of synthesis on quality, electronic properties and environmental stability of individual monolayer Ti_3C_2 MXene flakes. *Adv. Electron. Mater.* **2016**, *2*, 1600255. [CrossRef]
46. Vahid Mohammadi, A.; Moncada, J.; Chen, H.; Kayali, E.; Orangi, J.; Carrero, C.A.; Beidaghi, M. Thick and freestanding MXene/PANI pseudocapacitive electrodes with ultrahigh specific capacitance. *J. Mater. Chem. A* **2018**, *6*, 22123–22133. [CrossRef]
47. Yang, S.; Zhang, P.; Wang, F.; Ricciardulli, A.G.; Lohe, M.R.; Blom, P.W.M.; Feng, X. Fluoride-free synthesis of two-dimensional titanium carbide (MXene) using a binary aqueous system. *Angew. Chem. Int. Ed.* **2018**, *57*, 15491–15495. [CrossRef]
48. Zhao, Y.; Zhang, M.; Yan, H.; Feng, Y.; Zhang, X.; Guo, R. Few-layer large $Ti_3C_2T_x$ sheets exfoliated by $NaHF_2$ and applied to the sodium-ion battery. *J. Mater. Chem. A* **2021**, *9*, 9593–9601. [CrossRef]

49. Feng, A.; Yu, Y.; Wang, Y.; Jiang, F.; Yu, Y.; Mi, L.; Song, L. Two-dimensional MXene Ti_3C_2 produced by exfoliation of Ti_3AlC_2. *Mater. Des.* **2017**, *114*, 161–166. [CrossRef]
50. Levitt, A.S.; Alhabeb, M.; Hatter, C.B.; Sarycheva, A.; Dionb, G.; Gogotsi, Y. Electrospun MXene/carbon nanofibers as supercapacitor electrodes. *J. Mater. Chem. A* **2019**, *7*, 269–277. [CrossRef]
51. Huang, X.; Wu, P. A facile, high-yield, and freeze-and-thaw-assisted approach to fabricate MXene with plentiful wrinkles and its application in on-chip micro-supercapacitors. *Adv. Funct. Mater.* **2020**, *30*, 1910048. [CrossRef]
52. Mendoza-Sanchez, B.; Gogotsi, Y. Synthesis of two-dimensional materials for capacitive energy storage. *Adv. Mater.* **2016**, *28*, 6104–6135. [CrossRef] [PubMed]
53. Liu, T.; Liu, S.; Tu, K.H.; Schmidt, H.; Chu, L.; Xiang, D.; Martin, J.; Eda, G.; Ross, C.A.; Garaj, S. Crested two-dimensional transistors. *Nat. Nanotechnol.* **2019**, *14*, 223–226. [CrossRef] [PubMed]
54. Naguib, M.; Mashtalir, O.; Carle, J.; Presser, V.; Lu, J.; Hultman, L.; Gogotsi, Y.; Barsoum, M.W. Two-dimensional transition metal carbides. *ACS Nano* **2012**, *6*, 1322–1331. [CrossRef]
55. Lukatskaya, M.R.; Mashtalir, O.; Ren, C.E.; Dall'Agnese, Y.; Rozier, P.; Taberna, P.L.; Naguib, M.; Simon, P.; Barsoum, M.W.; Gogotsi, Y. Cation intercalation and high volumetric capacitance of two-dimensional titanium carbide. *Science* **2013**, *341*, 1502–1505. [CrossRef] [PubMed]
56. Yu, L.; Fan, Z.; Shao, Y.; Tian, Z.; Sun, J.; Liu, Z. Versatile N-doped MXene ink for printed electrochemical energy storage application. *Adv. Energy Mater.* **2019**, *9*, 1901839. [CrossRef]
57. Persson, I.; El Ghazaly, A.; Tao, Q.; Halim, J.; Kota, S.; Darakchieva, V.; Palisaitis, J.; Barsoum, M.W.; Rosen, J.; Persson, P.O.A. Tailoring structure, composition, and energy storage properties of MXenes from selective etching of in-plane, chemically ordered max phases. *Small* **2018**, *14*, 1703676. [CrossRef]
58. Wang, F.; Wu, X.; Yuan, X.; Liu, Z.; Zhang, Y.; Fu, L.; Zhu, Y.; Zhou, Q.; Wu, Y.; Huang, W. Latest advances in supercapacitors: From new electrode materials to novel device designs. *Chem. Soc. Rev.* **2017**, *46*, 6816–6854. [CrossRef]
59. Shao, Y.; El-Kady, M.F.; Sun, J.; Li, Y.; Zhang, Q.; Zhu, M.; Wang, H.; Dunn, B.; Kaner, R.B. Design and mechanisms of asymmetric supercapacitors. *Chem. Rev.* **2018**, *118*, 9233–9280. [CrossRef]
60. Zhong, C.; Deng, Y.; Hu, W.; Qiao, J.; Zhang, L.; Zhang, J. A review of electrolyte materials and compositions for electrochemical supercapacitors. *Chem. Soc. Rev.* **2018**, *44*, 7484–7539. [CrossRef]
61. Muzaffar, A.; Ahamed, M.B.; Deshmukh, K.; Thirumalai, J. A review on recent advances in hybrid supercapacitors: Design, fabrication and applications. *Renew. Sustain. Energy Rev.* **2019**, *101*, 123–145. [CrossRef]
62. Liu, H.; Liu, X.; Wang, S.; Liu, H.-K.; Li, L. Transition metal based battery-type electrodes in hybrid supercapacitors: A review. *Energy Storage Mater.* **2020**, *28*, 122–145. [CrossRef]
63. Lukatskaya, M.R.; Bak, S.-M.; Yu, X.; Yang, X.-Q.; Barsoum, M.W.; Gogotsi, Y. Probing the mechanism of high capacitance in 2D titanium carbide using in situ x-ray absorption spectroscopy. *Adv. Energy Mater.* **2015**, *5*, 1500589. [CrossRef]
64. Li, H.; Li, X.; Liang, J.; Chen, Y. Hydrous RuO_2-decorated MXene coordinating with silver nanowire inks enabling fully printed micro-supercapacitors with extraordinary volumetric performance. *Adv. Energy Mater.* **2019**, *9*, 1803987. [CrossRef]
65. Pan, Z.; Cao, F.; Hua, X.; Ji, X. A facile method for synthesizing CuS decorated Ti_3C_2 MXene with enhanced performance for asymmetric supercapacitors. *J. Mater. Chem. A* **2019**, *7*, 8984–8992. [CrossRef]
66. Wang, X.; Li, H.; Li, H.; Lin, S.; Ding, W.; Zhu, X.; Sheng, Z.; Wang, H.; Zhu, X.; Sun, Y. 2D/2D 1T-MoS_2/Ti_3C_2 MXene heterostructure with excellent supercapacitor performance. *Adv. Funct. Mater.* **2020**, *30*, 0190302. [CrossRef]
67. Wang, Y.; Dou, H.; Wang, J.; Ding, B.; Xu, Y.; Chang, Z.; Hao, X. Three-dimensional porous MXene/layered double hydroxide composite for high performance supercapacitors. *J. Power Source* **2016**, *327*, 221–228. [CrossRef]
68. Luo, Y.; Yang, C.; Tian, Y.; Tang, Y.; Yin, X.; Que, W. A long cycle life asymmetric supercapacitor based on advanced nickel-sulfide/titanium carbide MXene) nanohybrid and MXene electrodes. *J. Power Source* **2020**, *450*, 227694. [CrossRef]
69. Wen, Y.; Rufford, T.E.; Chen, X.; Li, N.; Lyu, M.; Dai, L.; Wang, L. Nitrogen-doped $Ti_3C_2T_x$ MXene electrodes for high-performance supercapacitors. *Nano Energy* **2017**, *38*, 368–376. [CrossRef]
70. Mu, X.; Wang, D.; Du, F.; Chen, G.; Wang, C.; Wei, Y.; Gogotsi, Y.; Gao, Y.; Dall'Agnese, Y. Revealing the pseudo-intercalation charge storage mechanism of MXenes in acidic electrolyte. *Adv. Funct. Mater.* **2019**, *29*, 1902953. [CrossRef]
71. Zhang, M.; Chen, X.; Sui, J.; Abraha, B.S.; Li, Y.; Peng, W.; Zhang, G.; Zhang, F.; Fan, X. Improving the performance of titanium carbide MXene in supercapacitor by partial oxidation treatment. *Inorg. Chem. Front.* **2020**, *7*, 1205–1211. [CrossRef]
72. Li, Z.; Ma, C.; Wen, Y.; Wei, Z.; Xing, X.; Chu, J.; Yu, C.; Wang, K.; Wang, Z.-K. Highly conductive dodecaborate/MXene composites for high performance supercapacitors. *Nano Res.* **2019**, *13*, 196–202. [CrossRef]
73. Li, K.; Wang, X.; Li, S.; Urbankowski, P.; Li, J.; Xu, Y.; Gogotsi, Y. An ultrafast conducting polymer@MXene positive electrode with high volumetric capacitance for advanced asymmetric supercapacitors. *Small* **2020**, *16*, 1906851. [CrossRef]
74. Zhang, C.J.; Anasori, B.; Seral-Ascaso, A.; Park, S.H.; McEvoy, N.; Shmeliov, A.; Duesberg, G.S.; Coleman, J.N.; Gogotsi, Y.; Nicolosi, V. Transparent, flexible, and conductive 2D titanium carbide (MXene) films with high volumetric capacitance. *Adv. Mater.* **2017**, *29*, 1702678. [CrossRef] [PubMed]
75. Zhao, W.; Peng, J.; Wang, W.; Jin, B.; Chen, T.; Liu, S.; Zhao, Q.; Huang, W. Interlayer hydrogen-bonded metal porphyrin frameworks/MXene hybrid film with high capacitance for flexible all-solid-state supercapacitors. *Small* **2019**, *15*, 1901351. [CrossRef]

76. Wu, X.; Huang, B.; Lv, R.; Wang, Q.; Wang, Y. Highly flexible and low capacitance loss supercapacitor electrode based on hybridizing decentralized conjugated polymer chains with MXene. *Chem. Eng. J.* **2019**, *378*, 122246. [CrossRef]
77. Qin, L.; Tao, Q.; El Ghazaly, A.; Fernandez-Rodriguez, J.; Persson, P.O.Å.; Rosen, J.; Zhang, F. High-performance ultrathin flexible solid-state supercapacitors based on solution processable $Mo_{1.33}C$ MXene and PEDOT:PSS. *Adv. Funct. Mater.* **2018**, *28*, 1703808. [CrossRef]
78. Shi, M.; Xiao, P.; Lang, J.; Yan, C.; Yan, X. Porous g-C_3N_4 and MXene dual-confined FeOOH quantum dots for superior energy storage in an ionic liquid. *Adv. Sci.* **2020**, *7*, 1901975. [CrossRef]
79. Tian, W.; Vahid Mohammadi, A.; Reid, M.S.; Wang, Z.; Ouyang, L.; Erlandsson, J.; Pettersson, T.; Wagberg, L.; Beidaghi, M.; Hamedi, M.M. Multifunctional nanocomposites with high strength and capacitance using 2D MXene and 1D nanocellulose. *Adv. Mater.* **2019**, *31*, 1902977. [CrossRef] [PubMed]
80. Wang, Y.; Wang, X.; Li, X.; Bai, Y.; Xiao, H.; Liu, Y.; Liu, R.; Yuan, G. Engineering 3D ion transport channels for flexible MXene films with superior capacitive performance. *Adv. Funct. Mater.* **2019**, *29*, 1900326. [CrossRef]
81. Quain, E.; Mathis, T.S.; Kurra, N.; Maleski, K.; van Aken, K.L.; Alhabeb, M.; Alshareef, H.N.; Gogotsi, Y. Direct writing of additive-free MXene-in-water ink for electronics and energy storage. *Adv. Mater. Technol.* **2019**, *4*, 1800256. [CrossRef]
82. Wang, Y.; Wang, X.; Li, X.; Liu, R.; Bai, Y.; Xiao, H.; Liu, Y.; Yuan, G. Intercalating ultrathin MoO_3 nanobelts into MXene film with ultrahigh volumetric capacitance and excellent deformation for high-energy-density devices. *Nano-Micro Lett.* **2020**, *12*, 115. [CrossRef] [PubMed]
83. Abdolhosseinzadeh, S.; Schneider, R.; Verma, A.; Heier, J.; Nuesch, F.; Zhang, C.J. Turning trash into treasure: Additive free MXene sediment inks for screen-printed micro-supercapacitors. *Adv. Mater.* **2020**, *32*, 2000716. [CrossRef] [PubMed]
84. Hu, H.; Hua, T. An easily manipulated protocol for patterning of MXenes on paper for planar micro-supercapacitors. *J. Mater. Chem. A* **2017**, *5*, 19639–19648. [CrossRef]
85. Zhang, J.; Seyedin, S.; Qin, S.; Wang, Z.; Moradi, S.; Yang, F.; Lynch, P.A.; Yang, W.; Liu, J.; Wang, X.; et al. Highly conductive $Ti_3C_2T_x$ MXene hybrid fibers for flexible and elastic fiber-shaped supercapacitors. *Small* **2019**, *15*, 1804732. [CrossRef]
86. Shao, W.; Tebyetekerwa, M.; Marriam, I.; Li, W.; Wu, Y.; Peng, S.; Ramakrishna, S.; Yang, S.; Zhu, M. Polyester@MXene nanofibers-based yarn electrodes. *J. Power Source* **2018**, *396*, 683–690. [CrossRef]
87. Chang, T.H.; Zhang, T.; Yang, H.; Li, K.; Tian, Y.; Lee, J.Y.; Chen, P.Y. Controlled crumpling of two-dimensional titanium carbide (MXene) for highly stretchable, bendable, efficient supercapacitors. *ACS Nano* **2018**, *12*, 8048–8059. [CrossRef] [PubMed]
88. Lipatov, A.; Lu, H.; Alhabeb, M.; Anasori, B.; Gruverman, A.; Gogotsi, Y.; Sinitskii, A. Elastic properties of 2D $Ti_3C_2T_x$ MXene monolayers and bilayers. *Sci. Adv.* **2018**, *4*, 491. [CrossRef]
89. An, H.; Habib, T.; Shah, S.; Gao, H.; Radovic, M.; Green, M.J.; Lutkenhaus, J.L. Surface-agnostic highly stretchable and bendable conductive MXene multilayers. *Sci. Adv.* **2018**, *4*, 118. [CrossRef] [PubMed]
90. Come, J.; Xie, Y.; Naguib, M.; Jesse, S.; Kalinin, S.V.; Gogotsi, Y.; Kent, P.R.C.; Balke, N. Nanoscale elastic changes in 2D $Ti_3C_2T_x$ (MXene) pseudocapacitive electrodes. *Adv. Energy Mater.* **2016**, *6*, 1502290. [CrossRef]
91. Shang, M.; Chen, X.; Li, B.; Niu, J. A fast charge/discharge and wide-temperature battery with a germanium oxide layer on a $Ti_3C_2T_x$MXene matrix as anode. *ACS Nano* **2020**, *14*, 3678–3686. [CrossRef] [PubMed]
92. Li, J.; Han, L.; Li, Y.; Li, J.; Zhu, G.; Zhang, X.; Lu, T.; Pan, L. MXene-decorated SnS_2/Sn_3S_4 hybrid as anode material for high-rate lithium-ion batteries. *Chem. Eng. J.* **2020**, *380*, 122590. [CrossRef]
93. Tang, X.; Liu, H.; Guo, X.; Wang, S.; Wu, W.; Mondal, A.K.; Wang, C.; Wang, G. A novel lithium-ion hybrid capacitor based on the aerogellikeMXene wrapped Fe_2O_3nanosphere anode and the 3D nitrogen sulphur dual-doped porous carbon cathode. *Mater. Chem. Front.* **2018**, *2*, 1811–1821. [CrossRef]
94. Ahmed, B.; Anjum, D.H.; Gogotsi, Y.; Alshareef, H.N. Atomic layer deposition of SnO_2 on MXene for Li-ion battery anodes. *Nano Energy* **2017**, *34*, 249–256. [CrossRef]
95. Cheng, R.; Wang, Z.; Cui, C.; Hu, T.; Fan, B.; Wang, H.; Liang, Y.; Zhang, C.; Zhang, H.; Wang, X. One-step incorporation of nitrogen and vanadium between $Ti_3C_2T_x$ MXene interlayers enhances lithium ion storage capability. *J. Phys. Chem. C* **2020**, *124*, 6012–6021. [CrossRef]
96. Ruan, T.; Wang, B.; Yang, Y.; Zhang, X.; Song, R.; Ning, Y.; Wang, Z.; Yu, H.; Zhou, Y.; Wang, D.; et al. Interfacial and electronic modulation via localized sulfurization for boosting lithium storage kinetics. *Adv. Mater.* **2020**, *32*, 2000151. [CrossRef]
97. Zhang, D.; Wang, S.; Li, B.; Yang, Y.G.S. Horizontal growth of lithium on parallelly aligned MXene layers towards dendrite-free metallic lithium anodes. *Adv. Mater.* **2019**, *31*, 1901820. [CrossRef]
98. Wei, C.; Fei, H.; Tian, Y.; An, Y.; Zeng, G.; Feng, J.; Qian, Y. Room-temperature liquid metal confined in MXene paper as a flexible, freestanding, and binder-free anode for next-generation lithium-ion batteries. *Small* **2019**, *15*, 1903214. [CrossRef]
99. Yang, Q.; Huang, Z.; Li, X.; Liu, Z.; Li, H.; Liang, G.; Wang, D.; Huang, Q.; Zhang, S.; Chen, S.; et al. A wholly degradable, rechargeable Zn-Ti_3C_2 MXene capacitor with superior anti-self-discharge function. *ACS Nano* **2019**, *13*, 8275–8283. [CrossRef] [PubMed]
100. Wang, S.; Wang, Q.; Zeng, W.; Wang, M.; Ruan, L.; Ma, Y. A new free-standing aqueous zinc-ion capacitor based on MnO_2–CNTs cathode and MXene anode. *Nano-Micro Lett.* **2019**, *11*, 70. [CrossRef]
101. Shi, J.; Wang, S.; Wang, Q.; Chen, X.; Du, X.; Wang, M.; Zhao, Y.; Dong, C.; Ruan, L.; Zeng, W. A new flexible zinc-ion capacitor based on δ-MnO_2@carbon cloth battery-type cathode and MXene@cotton cloth capacitor-type anode. *J. Power Source* **2020**, *446*, 227345. [CrossRef]